Variation in runoff generation and concentration-discharge behavior in three variably encroached grassland watersheds

by

Johnny Lee Pruitt III

B.S., University of Arkansas – Fort Smith, 2023

A THESIS

Submitted in partial fulfillment of the requirements for the degree

MASTER OF SCIENCE

Department of Geology

College of Arts and Sciences

KANSAS STATE UNIVERSITY

Manhattan, Kansas

2025

Approved by:

Major Professor:

Dr. Matthew Kirk

Copyright

Abstract

Displacement of grasses by woody plants, a phenomenon known as woody encroachment, is occurring in grasslands worldwide. Previous studies indicate woody encroachment has the ability to alter runoff generation, increase soil porosity and permeability, decrease soil water residence time, decrease streamflow, and even accelerate soil drying. However, little is understood about the consequences all of these processes have on streamflow sources and composition. To fill this knowledge gap, we deployed high-frequency sampling of stream water during seven different rainstorms during the 2024 water year from three variably-encroached watersheds hosting headwater streams at Konza Prairie Biological Station, a native tallgrass prairie in northeastern Kansas, USA. We also examined streamflow and precipitation records for two time periods, one before widespread encroachment occurred in any of the watersheds (1987-1990) and the other more recently (2020-2023), after significant encroachment. Woody encroachment varies between the watersheds primarily due to differences in the frequency of fire treatment. Upland and riparian woody plant coverage is 6% and 45%, respectively in the annually burned watershed, 20% and 70%, respectively in the biennially burned watershed, and 28% and 74%, respectively in the quadrennially burned watershed.

Isotope hydrograph separation analysis based on stream and precipitation stable isotope compositions did not reveal any clear differences in amounts of runoff generation between watersheds. Most of the storms that we sampled were not large enough to cause large changes in stream water isotope compositions. However, our analysis of stream discharge and precipitation records indicates that encroachment is decreasing the sensitivity of streamflow to storms. We examined discharge-precipitation relationships by normalizing the change in streamflow (ΔQ) to precipitation event size (P) and watershed area (A). Results show that $\Delta Q/P/A$ values were

higher in 2020-2023 than 1987-1990 for all three watersheds, but the difference was greatest for the least encroached watershed, potentially reflecting impacts of climate change on storm intensity coupled with changes in soil permeability as a result of encroachment. Moreover, an analysis of concentration-discharge behavior for stream solutes suggests that encroachment is altering stream composition. Both geogenic and biogenic solutes were more chemodynamic in the least encroached watershed compared to the more encroached watersheds. Additionally, the least encroached had lower pH and higher concentrations of alkalinity and bedrock weathering products, potential in response to encroachment-driven differences in the amount and depth of mineral weathering between watersheds.

Taken together, the findings of this study suggest that encroachment is impacting headwater streams not only in terms of their response to storms but also in terms of stream water composition, which can have significant downstream implications for flood risks and water quality.

Table of Contents

Table of Contents v
List of Figures vii
List of Tables x
Chapter 1 - Introduction 1
Chapter 2 - Study Area 5
Chapter 3 - Methods 11
  3.1 Field Methods 11
    3.1.1 Autosamplers 12
    3.1.2 Data Loggers 13
    3.1.3 Precipitation Collectors 13
    3.1.4 Weirs 14
  3.2 Laboratory Methods 14
  3.3 Calculations & Analysis 16
    3.3.1 Concentration-Discharge (C-Q) Analysis 16
    3.3.2 Isotope Hydrograph Separation 18
    3.3.3 Precipitation-Discharge (ΔQ/P/A) Analysis 18
Chapter 4 – Results 20
  4.1 Precipitation and Discharge 20
  4.2 Water Chemistry 24
  4.3 Concentration-Discharge Behavior 27
  4.4 Stable Water Isotopes 32
  4.5 Isotope Hydrograph Separation 35
Chapter 5 - Discussion 40
  5.1 Stream water sources 40
  5.2 Sources of solutes to streamflow 44
  5.3 Implications 48
  5.4 Limitations and future steps 49
Chapter 6 - Concluding Remarks 51
References 53

Appendix A - Concentration-Discharge Data 62
Appendix B - Precipitation-Discharge Data...63
Appendix C – Surface Water Geochemistry Calculations 64

List of Figures

Figure 1. *Conceptual model displaying the different flow pathways water can move throughout a watershed. Subsurface flow occurs below the surface through the varying layers of soil and bedrock. Overland flow occurs above the surface and through near surface soils, eventually discharging into the nearest water body or infiltrating into the surface. This model is sometimes referred to as the Shallow vs. Deep hypothesis.* *2*

Figure 2*. Location of the Konza Prairie Biological Station and watersheds N1B, N2B, and N4D highlighted. Blue triangles indicate weir locations where watershed discharge and sample collection for this study occurred.* *6*

Figure 3. *Average total precipitation by month from 2003 through 2023 for Konza Prairie. Majority of the precipitation occurs during the peak growing season running from April through September of each year. (Nippert, 2024).* *8*

Figure 4*. Average daily discharge by month for Konza Prairie watersheds N1B (blue), N2B (orange), and N4D (green) from 2003 through 2023. The majority of streamflow corresponds with the peak growing season, April through September of each year. (W. Dodds, 2024c, 2024b, 2024a)* *8*

Figure 5. *Partial stratigraphic column of the bedrock layers at Konza Prairie. The upper Eiss limestone, lower Eiss limestone, and Morrill limestone are significant contributors to stream water flow throughout the watersheds.* *9*

Figure 6*. Total daily precipitation (black bars), average daily discharge (blue line), and hourly samples rainstorms (red arrows) for each watershed (A) N1B, (B) N2B, and (C) N4D. *0.01 was added to each discharge to display no flow days on log scale.* *21*

***Figure** 7.* *Box plots for the change in discharge (peak discharge – antecedent discharge) divided by the amount of precipitation (normalized to watershed area) received for all hourly sampled events and events greater than 10mm during our study period for watersheds N1B, N2B, and N4D.* 22

Figure 8. *Box plots displaying the □Q/P/A analysis on all three watersheds (N01B blue, N02B red, N04D orange) during the years 1987-1990 (A) and 2020-2023 (B).* 23

Figure 9. *Box plots for alkalinity (A), pH* (B), fluoride (C), chloride (D), sulfate (E), sodium (F), potassium (K), magnesium (H), calcium (I), and strontium (J) concentrations for all surface water samples collected during the study period across all three watersheds. X marks the mean concentrations and dots mark outliers. *pH for events 1-5 only.* 26

Figure 10. *pH measured across all three watersheds every 5 minutes while flow was active. Gaps in data represent times when flow was not active or when instruments were not recording.* 27

Figure 11. *b parameter vs. CVc/CVq plots for all surface water samples collected at N1B (A), N2B (B), and N4D (C).* 30

Figure 12. *CQ slope (b parameter) vs. CVc/CVq plots for trace elements for event seven only at N2B (A) and N4D (B).* 31

Figure 13. *Stable water isotopes in all surface water and precipitation samples collected during the study. The solid orange line indicates the Global Meteoric Water Line (GMWL) and the solid blue line indicates the Local Meteoric Water Line (LMWL). Graphs displaying data for (A) all samples collected, (B) samples in event one, (C) event two, (D) event three, (E) event four, (F) event five, (G) event six, and (H) event seven.* 34

Figure 14. *Percentage of event water vs. time for (A) event one, (B) event two, (C) event three, (D) event four, (E) event five, (F) event six, and (G) event seven.* *37*

List of Tables

Table 1. *Percentage of woody plant coverage within the different areas of our study watersheds. Upland refers to areas on hillslopes and near hill peaks. Riparian refers to the areas within 30m of the first order streams found within the watersheds. (Dodds et al., 2023).* . 7

Table 2. *List of hourly sampled rainstorms (1 - 7), the date each event occurred, and the number of samples collected from each watershed during the event (including precipitation samples).* 11

Table 3. *Total discharge from each watershed during our study period (April 30th - July 11th), the depth of the catchment that amount of discharge could cover (mm), the percentage of precipitation the catchment coverage accounts for, and the dates where streamflow was active.* 20

Table 4. *Mean, median, standard deviation (St. Dev.), number of storms (n), and p values for ΔQ/P/A analysis for years 1987-1990 and 2020-2023.* 23

Table 5. *Stable water isotope values used for end-member mixing calculations for event water and pre-event water. All isotopic values are in ‰ VSMOW.* 36

Table 6. *Hydrologic characteristics for hourly sampled events analyzed for isotope hydrograph separation. fQ_e is the maximum fraction of event water during the storm, Q_e is the maximum discharge of event water during each storm, P is the amount of precipitation received, aQ is the antecedent discharge, and dQ is the maximum change in discharge during the event* 39

Chapter 1 - Introduction

Grasslands and the native vegetation found within them represent nearly forty percent of terrestrial land coverage worldwide and can be majorly impacted by land-use changes and climate disturbances (Blair et al., 2014). The type of vegetation coverage within a grassland can have profound effects on the hydrology of the environment, altering infiltration rates, the amount of evapotranspiration occurring, and surface water groundwater interactions (Dodds et al., 2023; Sadayappan et al., 2023). Woody plant species such as the American plum (*P. americana*) and the eastern red cedar (*Juniperus virginiana*) have been observed rapidly expanding and outcompeting native grasslands for decades in a process known as woody plant encroachment, or simply just woody encroachment. Historically only mainly occurring within the riparian zone of grasslands, woody encroachment has been observed expanding outside of those traditional areas globally, potentially altering the hydrology of one of earth's largest biomes. Within this study, we aim to investigate how woody encroachment may alter streamflow sources and runoff mechanisms during rainstorms in order to better understand woody encroachment's effects on grassland headwater streamflow chemistry.

Precipitation can contribute to streamflow through two main mechanisms, subsurface flow and overland flow. Subsurface flow (***Fig. 1***) is the portion of precipitation that infiltrates the ground surface, sometimes called groundwater flow or interflow, and can eventually be introduced as streamflow via a spring or groundwater seepage. Overland flow (***Fig. 1),*** sometimes called runoff, is the portion of precipitation that does not infiltrate the surface and instead flows over it and is directly added as streamflow (Stewart et al., 2022).

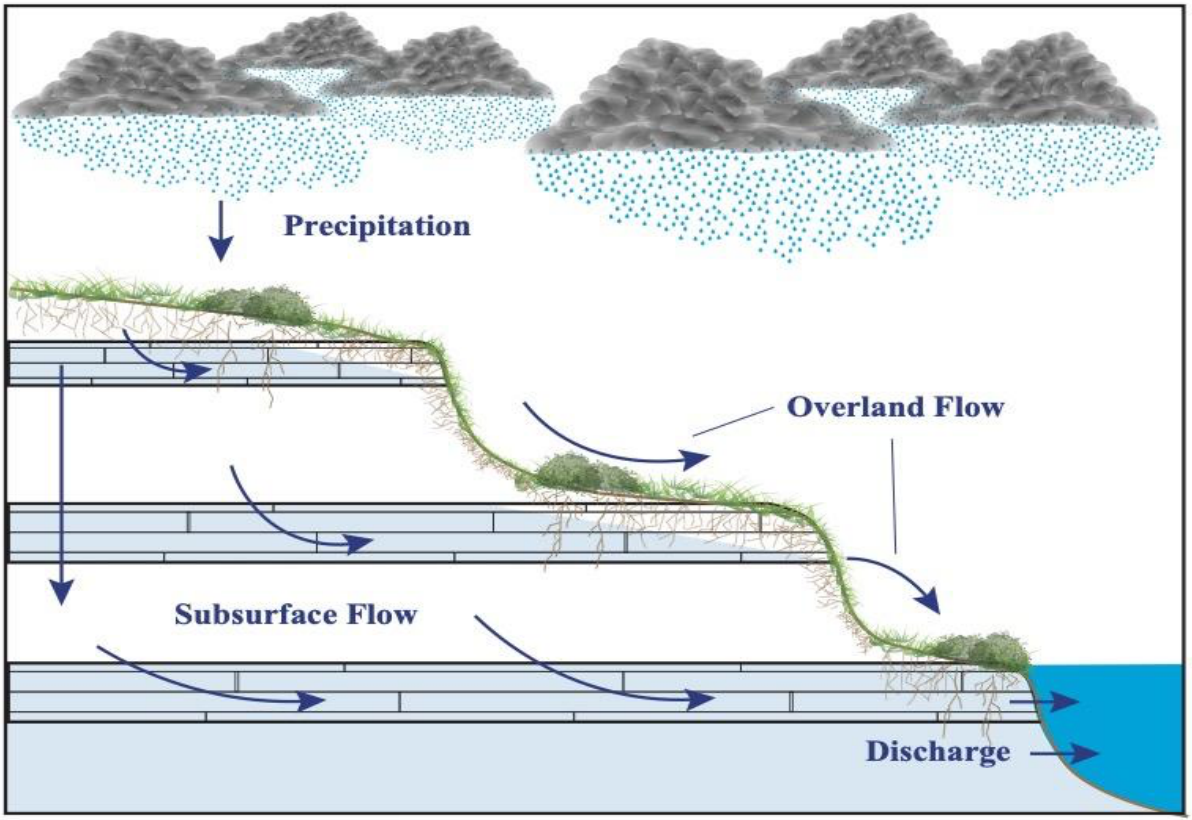

Figure 1. *Conceptual model displaying the different flow pathways water can move throughout a watershed. Subsurface flow occurs below the surface through the varying layers of soil and bedrock. Overland flow occurs above the surface and through near surface soils, eventually discharging into the nearest water body or infiltrating into the surface. This model is sometimes referred to as the Shallow vs. Deep hypothesis.*

Precipitation can contribute to both overland flow and subsurface flow, however differing conditions can cause precipitation to contribute to one more than the other. If the rate of water input (i.e., precipitation) exceeds that of the infiltration rate, it will cause the excess water to run across the land surface as overland flow, a process known as infiltration-excess overland flow (Steenhuis et al., 2023). If the underlying rock or soil is already fully saturated, then additional infiltration is not possible, this is known as saturation-excess overland flow (Steenhuis et al., 2023). In addition to these two determinants, other factors such as surface slope, surface conditions, and vegetation coverage can also influence the proportions of runoff and infiltration during a storm.

With regard to vegetation, woody plant species and shrubs tend to have larger root systems that reach down further into the subsurface than those of native C_4 grasses (O'Keefe et al., 2019; Ratajczak et al., 2011), potentially creating pathways for water to flow during rainstorms. Previous studies have shown that woody encroachment can alter soil permeability (Qiao et al., 2017), increase the relative contributions of deeper inputs to streams (Sadayappan et al., 2023), alter groundwater recharge (Kharel et al., 2018), and decrease streamflow (Dodds et al., 2023). During rainstorms, the deep subsurface pathways created by woody plant species roots have the potential to enhance the contribution of groundwater inputs to streamflow, thereby reducing the amount of runoff contributed (Jarecke et al., 2025; Qiao et al., 2017).

Sullivan et al., (2019) hypothesized that fine grassland root systems encourage lateral interflow, whereas larger woody species' root systems promote deeper vertical interflows. Because woody species' root systems are typically larger and infiltrate much deeper, it is suggested that precipitation is more likely to infiltrate deeper and become groundwater as opposed to runoff. Qiao et al., (2017) observed that watersheds affected by eastern redcedar encroachment (75% canopy coverage) experienced an average decrease of 22 mm in total annual runoff -- a 3% reduction -- compared to grassland watersheds. Additionally, these researchers observed a shift from saturation-excess overland flow in grassland watersheds to infiltration-excess overland flow in encroached watersheds (Qiao et al., 2017). This shift is likely due to the aforementioned deep root systems of woody plant species and their ability to drive precipitation deeper into the subsurface. Although itis clear that woody encroachment has the ability to alter porosity, hydrologic connectivity, and runoff generation mechanisms, little is understood about how those affects ultimately impact streamflow chemistry.

According to the shallow vs. deep hypothesis (***Fig. 1***), streamflow chemistry is derived from the culmination of various water sources and their respective chemical compositions, all found within the watershed (Stewart et al., 2022). Baseflow, which is the flow of stream water during "normal" conditions, is sustained by groundwater inputs from aquifers, therefore streamflow chemistry during this time mirrors that of the local groundwater. During high-flow, when precipitation is occurring, discharge is near its peak, and conditions are typically saturated, streamflow chemistry typically mirrors that of soil water and precipitation. Groundwater is usually enriched with base cations commonly found with bedrock weathering whereas soil water is enriched with organic materials associated with biological life (Stewart et al., 2022). Because woody plant encroachment has the ability to alter near surface hydrological processes and increase deep water inputs, we expect that streamflow chemistry will reflect those transitions.

If woody encroachment is altering streamflow chemistry, we would expect to see variations in solute concentration behaviors across watersheds with varying degrees of encroachment. Concentration-discharge (C-Q) behaviors, which is how solute concentrations change with altering discharge, can be significantly altered due to biological process from plants and other lifeforms (Speir et al., 2023). Variations in biological life has the ability to alter C-Q behaviors directly through altering solute concentrations and altering discharge via the hydrological budget (Speir et al., 2023). Woody plant species can transpire nearly twice as much water into the atmosphere as compared to native C_4 grasses (O'Keefe et al., 2020), ultimately altering the hydrological budget of the watershed and potentially affecting discharge. By altering the concentration of solutes within the watershed and changing streamflow discharge, woody plant encroachment may have profound impacts on streamflow chemistry that has yet to be realized or quantified.

Chapter 2 - Study Area

The Konza Prairie Biological Station is a Long-Term Ecological Research (LTER) site located within the Flint Hills region of northeastern Kansas, USA. The site was originally established in the 1970's through generous donations and hard work by the Nature Conservancy and Kansas State University faculty. The site has been used to better understand and research hydrological connectivity, environmental alterations, nutrient cycling, land-use practices, and other ecological processes (Hulbert, 1985). The 8,600-acre site offers researchers and environmental scientists the opportunity to study environments that have remained relatively untouched by modern humans, a unique research opportunity. Currently, there are roughly sixty different watersheds located at Konza Prairie, each with different treatments including fire regiments and grazing practices. This study focuses on three nearly identical watersheds at Konza Prairie with each experiencing differing degrees of woody encroachment.

The three watersheds investigated in this study, (***Fig. 2***) N1B, N2B, and N4D, border each other geographically, feature nearly identical underlying bedrock, are freely grazed by bison, and each has an intermittent headwater stream flowing through them. The key difference between the three watersheds is how the land is managed via prescribed burning. Prescribed burning of the tallgrass prairie is a natural land management practice that can help remove dead plant material, promote new plant growth, release nutrients into the system, and eliminate or control invasive species (Dickson et al., 2019). Konza Prairie staff conduct prescribed burns each spring in the study watersheds and the number in each watershed title corresponds to its burn frequency. N1B is burned yearly, N2B is burned biannually, and N4D is burned every four years.

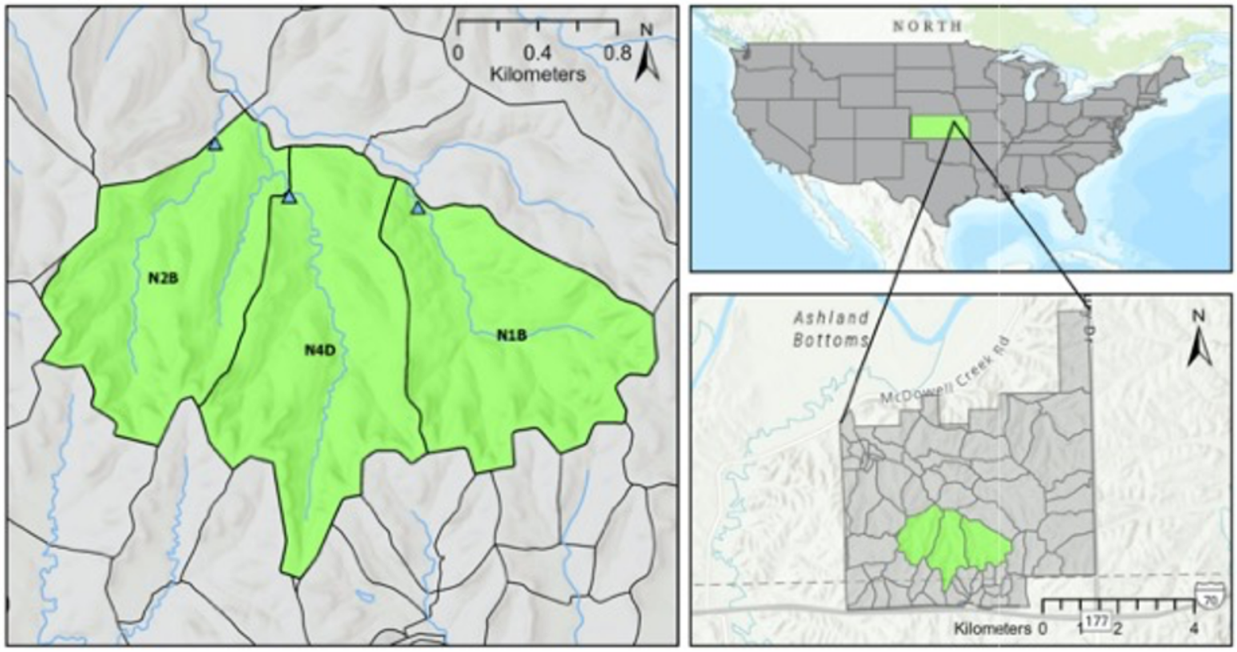

Figure 2. *Location of the Konza Prairie Biological Station and watersheds N1B, N2B, and N4D highlighted. Blue triangles indicate weir locations where watershed discharge and sample collection for this study occurred.*

One of the main controls on woody expansion in the study area is burn frequency, (Dodds et al., 2023). Since the establishment of Konza Prairie, woody plant species such as rough-leaf dogwood (*Cornus drummondi*) and smooth sumac (*Rhus glabra*) have been observed expanding up onto the hillslopes of the watersheds, past their historical range of just within the riparian zone (Dodds et al., 2023; Ratajczak et al., 2011; Veach et al., 2014). Recent research across Konza Prairie observed woody encroachment increasing with decreasing fire frequency (Dodds et al., 2023; Keen et al., 2024). The study by Dodds et al. (2023) tested woody vegetation removal in watersheds N2B as a means of testing the impact of woody encroachment on streamflow (Dodds et al., 2023). Currently, these three watersheds are nearly identical with the exception of the amount of woody plant encroachment, which offers up the unique ability for us to research the effects of the phenomena further.

Table 1. *Percentage of woody plant coverage within the different areas of our study watersheds. Upland refers to areas on hillslopes and near hill peaks. Riparian refers to the areas within 30m of the first order streams found within the watersheds. (Dodds et al., 2023).*

	N1B	**N2B**	**N4D**
Upland	6%	20%	27.5%
Riparian	45%	70%	74%

On average, Konza Prairie receives 835 mm of precipitation annually with roughly 75% of it falling during the peak growing season running from April through September (Hayden, 1998). Discharge from our three watersheds mostly coincides with the amount of precipitation received, however the window is slightly shorter than that of the growing season. Although precipitation follows a nice bell-shaped pattern peaking in June ***(Fig. 3)***, discharge across the three watersheds does not follow that same trend (***Fig. 4***). Discharge peaks in May or June but then quickly falls off in the month of July for all three watersheds, this is likely due to evapotranspiration rates reaching their maximum and plants pulling more water away from streamflow (O'Keefe et al., 2020). Up to 75% of the total water budget at Konza Prairie attributed to evapotranspiration (Steward et al., 2011).

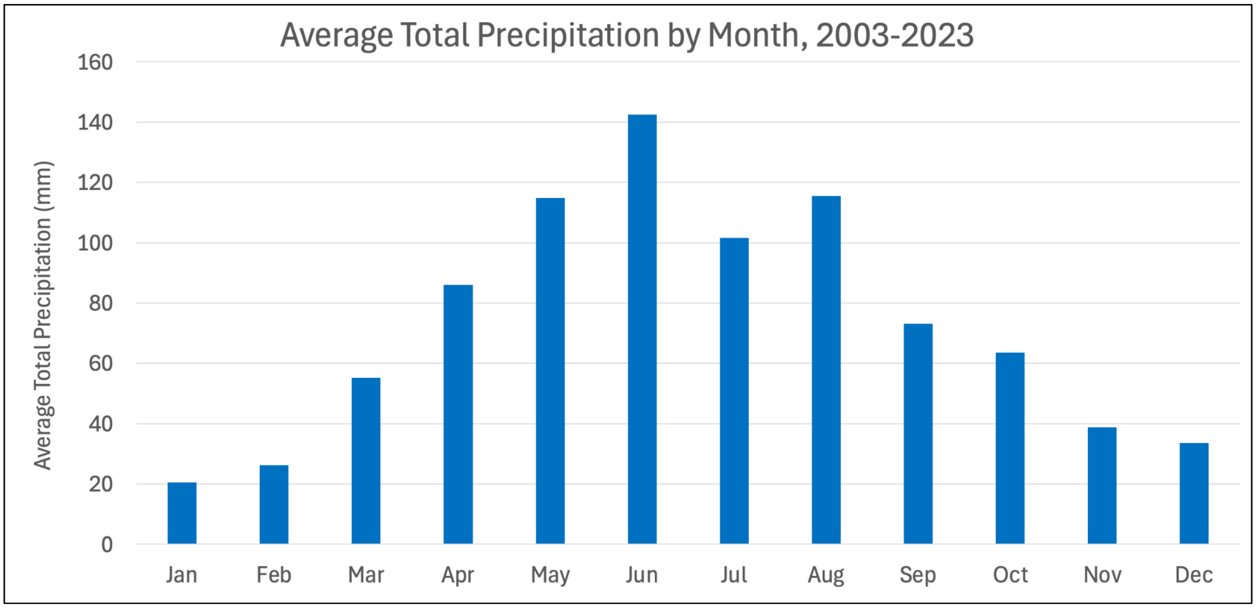

Figure 3. *Average total precipitation by month from 2003 through 2023 for Konza Prairie. Majority of the precipitation occurs during the peak growing season running from April through September of each year. (Nippert, 2024).*

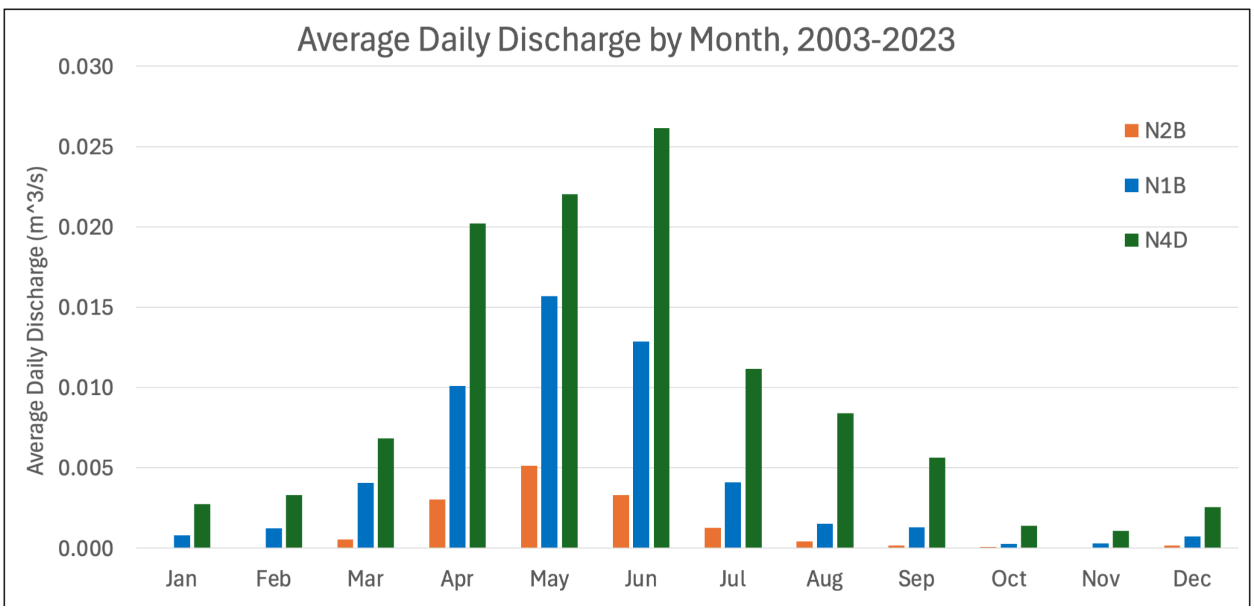

Figure 4*. Average daily discharge by month for Konza Prairie watersheds N1B (blue), N2B (orange), and N4D (green) from 2003 through 2023. The majority of streamflow corresponds with the peak growing season, April through September of each year. (W. Dodds, 2024c, 2024b, 2024a).*

The distinct rolling hillslopes of Konza Prairie were formed over millions of years by the headwater tributaries of the Kansas River (Oviatt, 1998). These headwater streams cutting through the landscape erode away the underlying Permian sedimentary rocks including limestones, mudstones, shales, and paleosols. The shallowest underlying bedrock at Konza Prairie consists primarily of alternating, nearly horizontal layers of limestone (1-2 meters thick) and shales (3-4 meters thick) (***Fig. 5***). These underlying rock layers are important contributors and controllers of Konza Prairie hydrology. The limestone layers hold water and act as perched aquifers where groundwater can flow horizontally and vertically, whereas the shale layers act as aquitards, restricting vertical flow, although some limited flow through cracks is likely occurring (Macpherson, 1996). Many of these limestone and shale layers terminate in the streams in each watershed, making them major stream water sources.

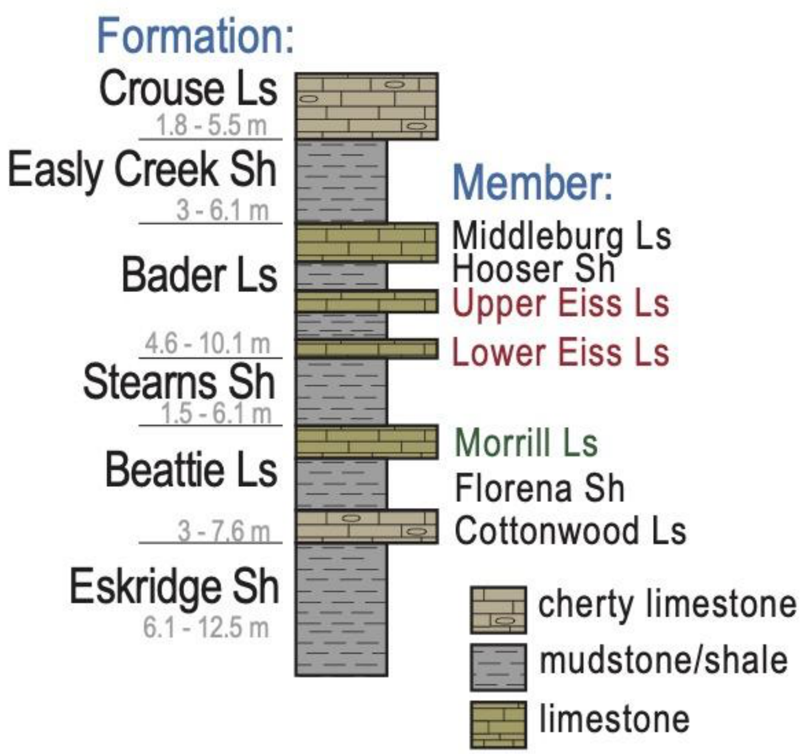

Figure 5. *Partial stratigraphic column of the bedrock layers at Konza Prairie. The upper Eiss limestone, lower Eiss limestone, and Morrill limestone are significant contributors to stream water flow throughout the watersheds.*

Sullivan et al., (2019) used mixing calculations at Konza Prairie to determine that streamflow consists of four major contributors: surface runoff, soil water, groundwater from carbonate aquifers, and groundwater flowing along the carbonate-shale layer contacts. In a follow up study, Hatley et al., (2023) used mixing calculation to show that streamflow in N4D is dominantly supplied by groundwater inputs sourced from the thin carbonate aquifers.

Chapter 3 - Methods

3.1 Field Methods

To characterize the effects of woody encroachments on streamflow sourcing, we needed to be able to monitor stream conditions and collect samples across the three watersheds (N1B, N2B, & N4D) simultaneously during rainstorms. To accomplish our goals, we deployed a YSI Prosample P autosampler, HOBO pH logger, and precipitation collector to each watershed. The instruments were located within 15 meters upstream or downstream of the weirs in each watershed. We conducted sampling from 04/30/2024 to 07/11/2024 to coincide with the wet season, when streamflow is most consistent. Ultimately, we sampled seven storm events that were anticipated based on weather forecasts to be of decent size and duration. Our goal was to begin sampling before (1-3 hours) precipitation began and stop after (1-3 hours) the precipitation ended. In total, 268 samples of stream water and precipitation were collected over the 92-day sampling period.

Table 2. *List of hourly sampled rainstorms (1 - 7), the date each event occurred, and the number of samples collected from each watershed during the event (including precipitation samples).*

Event	Dates	N1B	N2B	N4D
		samples	samples	samples
1	05/01-05/02	22	23	-
2	05/06-05/07	11	11	11
3	06/02	11	11	-
4	06/07-06/08	14	14	14
5	06/08-06/09	15	15	15
6	06/18-06/19	25	-	24
7	07/03-07/04	-	16	16

3.1.1 Autosamplers

The YSI Prosample P is a portable automatic sampler capable of collecting stream samples at pre-programmed intervals. An autosampler was placed on the stream bank near each watershed's weir. The autosamplers were attached to a large tree via vinyl coated wire rope to ensure the instruments' safety during large storm events or encounters with Bison. Attached to the peristaltic pump was a 5m long suction hose with a pre-installed sinker weight on the end, each hose was secured to the streambeds via metal stakes. The end of the hose, with the pre-installed sinker weight, was laid on the bottom of the streambed that consistently received upstream water input and featured good flow. On the other side of the peristaltic pump, within the autosamplers housing, is an automated distributor arm that can choose various bottles to place the stream sample into. The bottom of each autosampler contained 24 individual 1L polyethylene bottles that were labeled with each watershed and assigned a bottle number, 1-24. The housing of the autosampler features an arrow that indicates its start position of the distributor arm. Each autosampler was programmed to take one 500mL sample each hour from the stream, starting at a desired time.

Before each storm event newly charged batteries would be placed in each autosampler and the program would be set to start sampling at a desired time. Since all three autosamplers were programmed with the same time and date, each could take samples simultaneously, giving us a snapshot of the stream water in each watershed at the exact same time. The autosamplers would take one 500mL sample every hour until the program was ended by the user. Once finished, the polyethylene containers were capped and taken back to the Aqueous Geochemistry Lab at Kansas State University and refrigerated until lab processing could take place.

3.1.2 Data Loggers

The HOBO pH and Temperature Data Logger is a long-term monitoring device designed to measure pH and temperature of water at pre-set time intervals. The data logger also needs to be calibrated for pH at least once a week, this was completed by the researchers within the field at least once a week, or before a sampled precipitation event, whichever came first. The logged data was also collected at the time of calibration. A calibration was considered successful if the measured pH was within 0.05pH of the standard 7.01pH solution. For our study, the data loggers were suspended within the streamflow via PVC tubing and short metal fence posts. pH and temperature were measured every five minutes during our sampling period for each of the three watersheds, regardless of if a precipitation event was anticipated.

3.1.3 Precipitation Collectors

In order to determine how much of the streamflow is sourced from subsurface flow and overland flow, we needed to collect precipitation samples for analysis. A ball-in-funnel type collector was used using ping-pong balls with mesh netting covering the top of the funnel (Scholl, 2018). With this design, evaporation is minimized as the ball floats when water is input but seals the funnel when precipitation is not occurring. 1L bottles capped with rubber stoppers drilled to fit the funnels were used in this study. The collectors were fitted to fencing surrounding the weirs of the watershed. The precipitation samples were collected after each event and taken to the laboratory for storage and subsequent analysis. The precipitation collectors were rinsed with DI water after each use.

Precipitation loggers were also deployed by the Division of Biological Sciences at Kansas State University. These HOBO loggers measure precipitation amounts once every hour. For this study, we used one HOBO logger located near the N1B weir for its calculations. Since

N2B does not have a HOBO logger near its weir, we used the one located at N4D's weir for the calculations involving both N4D and N2B (Nippert, 2024). These weirs are geographically close to each other and are likely to experience only small differences in precipitation.

3.1.4 Weirs

Konza Prairie Biological Station currently has 4 v-notch weirs that measure stream discharge in m^3/s every five minutes (Dodds, 2024a, 2024b, 2024c). These weirs are operated and maintained by Konza Prairie staff and researchers at Kansas State University. The stream gauges at Konza Prairie use a bubble type mechanism that is used to measure the stream stage, or the water height. Once the water height is known, it is compared to an established mathematical relationship to determine what the discharge was at that time. This study was not directly involved with the collection of these data; however, we are grateful for the valuable hydrologic information.

3.2 Laboratory Methods

In the laboratory, surface water samples were taken out of refrigeration in sets of four to be filtered and stored. The surface water samples were filtered using suction filtration with a 0.45μm paper filter. The amount of water filtered was measured and later compared to the dry weight of each filter to determine sediment load in mg/L. Once filtered, each sample was separated into five distinctly labeled bottles and any remaining sample water was discarded. The five bottles included one 60mL HDPE bottle for alkalinity and major anion analysis, one 60mL HDPE bottle for major cation analysis, one 40mL glass vial for non-purgeable organic carbon (NPOC) and total dissolved nitrogen (TN) analysis, one 2mL glass vial for stable water isotope analysis, and one 125mL HDPE bottle for extra sample storage. Additionally, all precipitation samples were filtered using syringes fitted with 40µm disc filters and stored in labeled glass vials.

Anion samples were immediately placed back into refrigeration after filtration. Alkalinity was measured from the anion sample bottles in all surface water samples using end-point (pH 4.5) titrations with a ThermoScientific OrionStarT910 pH Titrator equipped with 0.02 N H_2SO_4 (sulfuric acid) as the titrant. Once complete, samples were again refrigerated until major anion analysis could be completed. Major anion concentrations (F^-, Cl^-, NO^{2-}, Br^-, NO_3^-, and SO_4^{2-}) were measured using a ThermoScientific ICS-1100 Ion Chromatograph (IC) instrument.

Cation samples were immediately preserved with 20µL of trace metal grade HNO_3 (nitric acid) and stored at room temperature after filtration. Major cation concentrations (Na^+, NH_4^+, K^+, Mg^{2+}, Ca^{2+}, Sr^{2+}) were measured using a ThermoScientific ICS-1100 Ion Chromatograph (IC) instrument.

Trace element concentrations (Uranium (Ur), Barium (Br), Rubidium (Rb), Lanthanum (La), Phosphorus (P), Manganese (Mn), Strontium (Sr), Boron(B), Copper (Cu), Iron (Fe), and Arsenic (As)) were measured for event seven with coordination of the Earth, Environment, and Resource Sciences department at the University of Texas at El Paso. Inductively Coupled Plasma Mass Spectrometry (ICP-MS) was used to analyze the samples, and results were reported in parts-per billion (ppb).

NPOC samples were immediately preserved with 20µL of HCl (hydrochloric acid) and placed back into refrigeration after filtration. NPOC and TN were later measured using a Shimadzu TOC-L total organic carbon analyzer.

We sent all surface water and precipitation samples to the Stable Isotope Mass Spectrometry Laboratory at the Kansas State University Division of Biology to measure stable water isotopes, $\delta^{18}O$ and δD. Results are presented as per mil (‰) relative to Vienna Standard Mean Ocean Water (VSMOW).

The 125mL nalgene bottle collected for extra sample storage was frozen for optimal preservation. All samples were filtered, stored, and then analyzed within one month of collection. The 1L polyethylene autosampler bottles were thoroughly rinsed with DI water before returning to the field.

3.3 Calculations & Analysis

3.3.1 Concentration-Discharge (C-Q) Analysis

We evaluated concentration-discharge (C-Q) relationships for all the major ions measured in each stream to better understand how water flow pathways may differ between the watersheds. C-Q analysis provides a solid quantitative analysis that is useful for making speculations about flow pathways transporting solutes within a watershed (Hatley et al., 2023; Sullivan, Stops, et al., 2019a). Chemostatic solutes are those that remain relatively constant in concentration as discharge widely fluctuates, this behavior is common for mineral weathering solutes such as Ca^{2+}, Mg^{2+}, SiO_2^{2-}, and for total nitrogen and phosphorus within agricultural settings. Chemodynamic solutes are those whose concentrations fluctuate along with discharge. Two common behaviors of chemodynamic solutes are flushing and dilution. Flushing (sometimes called mobilization) occurs when concentrations of a solute increase with increasing discharge, and dilution occurs when the concentration of a solute decreases with increasing discharge (Stewart et al., 2022). Many previous studies have shown that C-Q relationships are complex, they however offer unique insight into the geochemistry occurring within an environment.

To quantify the C-Q behavior of solutes, we first calculated the ‘b’ component in the power law relationship (Equation 1):

$$C = aQ^b \tag{1}$$

Where *C* is the solute's measured concentration, *Q* is discharge, and *a* and *b* are constants derived from the regression. When concentration and discharge are plotted on a log-log scale, the slope of the best fit line is *b*. A slope near zero represents chemostatic behavior, whereas a slope not equaling zero represents chemodynamic behavior (Speir et al., 2023). A negative slope ($b<0$) is consistent with dilution of a solute during increasing stream discharge whereas a positive slope ($b>0$) represents flushing, the increase in solute concentration with increasing stream discharge.

Secondly, we also assessed the variability of each solute using by ratioing the coefficients of variation in concentration and discharge, as shown below (Equation 2).

$$\frac{CV_C}{CV_Q} = \frac{\frac{\sigma_C}{\mu_C}}{\frac{\sigma_Q}{\mu_Q}} = \frac{\sigma_C \mu_Q}{\sigma_Q \mu_C} \tag{2}$$

Where CV is the ratio of the coefficients of variation between the solute and discharge, σ is the standard deviation, and μ is the mean of the solute concentration (C) and stream discharge (Q) (Speir et al., 2023). For this analysis, low variability represents chemostatic behavior ($\frac{CV_C}{CV_Q} > 0$), and chemodynamic behavior is represented by higher variability.

Following many previous studies, we combined these two approaches by plotting $\frac{CV_C}{CV_Q}$ on the x-axis and *b* on the y-axis (Hatley et al., 2023; Sullivan et al., 2019, Speir et al., 2023). This approach allows us to better visualize how solutes are changing with discharge, when $\frac{CV_C}{CV_Q}$ is near zero, it represents chemostatic behavior, however as it approaches one it represents chemodynamic behavior. The y-axis value (b) indicates whether the solute is acting in a flushing or dilution manner, with more positive b values represent flushing and more negative b values represent dilution. Some solutes are highly variable and will not correlate with discharge, this is represented as "Highly Reactive Solutes."

3.3.2 Isotope Hydrograph Separation

We calculated the proportions of runoff and baseflow in the stream water of each watershed using a method known as isotope hydrograph separation. Using chemical tracers $\delta^{18}O$ and δD, we are able to quantitatively assess the contributions to streamflow from a multitude of different sources using the following equations (Equation 3):

$$X_M = X_A f_A + X_B f_B + \ldots + X_n f_n$$

$$f_A + f_B + \ldots + f_n = 1 \tag{3}$$

In the above equations, X represents the different chemical tracers used ($\delta^{18}O$ and δD) subscript M represents mixed water, the other subscripts (A, B, … n) represent the different endmembers present, and finally f represents the fractional contribution of each endmember to the mixed water. Previous research on N4D stream water has shown that it is primarily supplied by four different sources, direct precipitation into the stream, soil water flow, overland flow, and subsurface flow (Hatley et al., 2023; Keen et al., 2023; Sullivan, Stops, et al., 2019a). For this study, however, we simply separated runoff and baseflow into two distinct groups via pre-event water and event water, allowing us to consider the impact of encroachment on surface and subsurface flow partitioning.

3.3.3 Precipitation-Discharge (ΔQ/P/A) Analysis

Precipitation total (P), antecedent discharge (aQ), and the difference between peak discharge and the antecedent discharge (ΔQ) for all sampled events or when precipitation was greater than 10mm during the wet season (April 1-August 1, 2024) was analyzed to better understand runoff generation. Additionally, we divided the difference in discharge (ΔQ) by the total amount of precipitation to better understand how each watershed behaves ($\Delta Q/P$), we also divided each calculated value by the watershed area (A) to normalize them ($(\Delta Q/P)/A$).

Although this analysis cannot directly measure saturation of each watershed or runoff generation, it provides a unique look at how much each stream swelled given similar precipitation amounts, producing a rough qualitative look at how each stream reacts to disturbances. To better understand how these watersheds behavior may have changed over time, we used historical data from Konza Prairie to conduct the same analysis and compare those results with our 2024 analysis. We chose to analyze the first four years these data were collected (1987-1990) and the four most recent years of data collection (2020-2023). Note, this analysis was only performed when more than 10 mm of rainfall occurred ***and*** streamflow was active, any events where one of these two statements is not true was excluded from the analysis.

Chapter 4 – Results

Data collected within this study has been submitted for publication to the Konza Prairie Biological Station's online database, all surface water geochemistry data collected is available for use by others (Pruitt & Kirk, 2025).

4.1 Precipitation and Discharge

During our study period (April 30th – July 11th), 372 mm of precipitation was received, of which 270 mm (73%) fell during just six individual events (***Fig. 6***). The largest precipitation event of the year (63 mm on 4-25-24) initiated streamflow and coincides with the highest discharge across the three watersheds, (5.36, 0.73, and 2.04 m^3/s across N1B, N2B, and N4D respectively). Once flowing, we observed large variations in total streamflow discharge with the largest amount of discharge occurring at N4D and the smallest at N2B. Average daily discharge gradually decreases in each watershed thereafter, with the occasional increase following large rainstorms. Discharge at the weirs temporarily stopped towards the end of June at all three watersheds due to drying but was resumed once large rainstorms occurred.

Table 3. *Total discharge from each watershed during our study period (April 30th - July 11th), the depth of the catchment that amount of discharge could cover (mm), the percentage of precipitation the catchment coverage accounts for, and the dates where streamflow was active.*

	N1B	N2B	N4D
Total Discharge (m^3)	66,570	20,090	107,900
Catchment Coverage (mm)	55.48	16.88	79.95
% of Precipitation	14.94	4.54	21.52
Duration of Streamflow	4/25/24 - 6/22/24 6/28/24 – 7/25/24	4/25/24 – 6/11/24 7/1/24 – 7/19/24	4/25/24 – 6/25/24 6/28/24 – 8/23/24

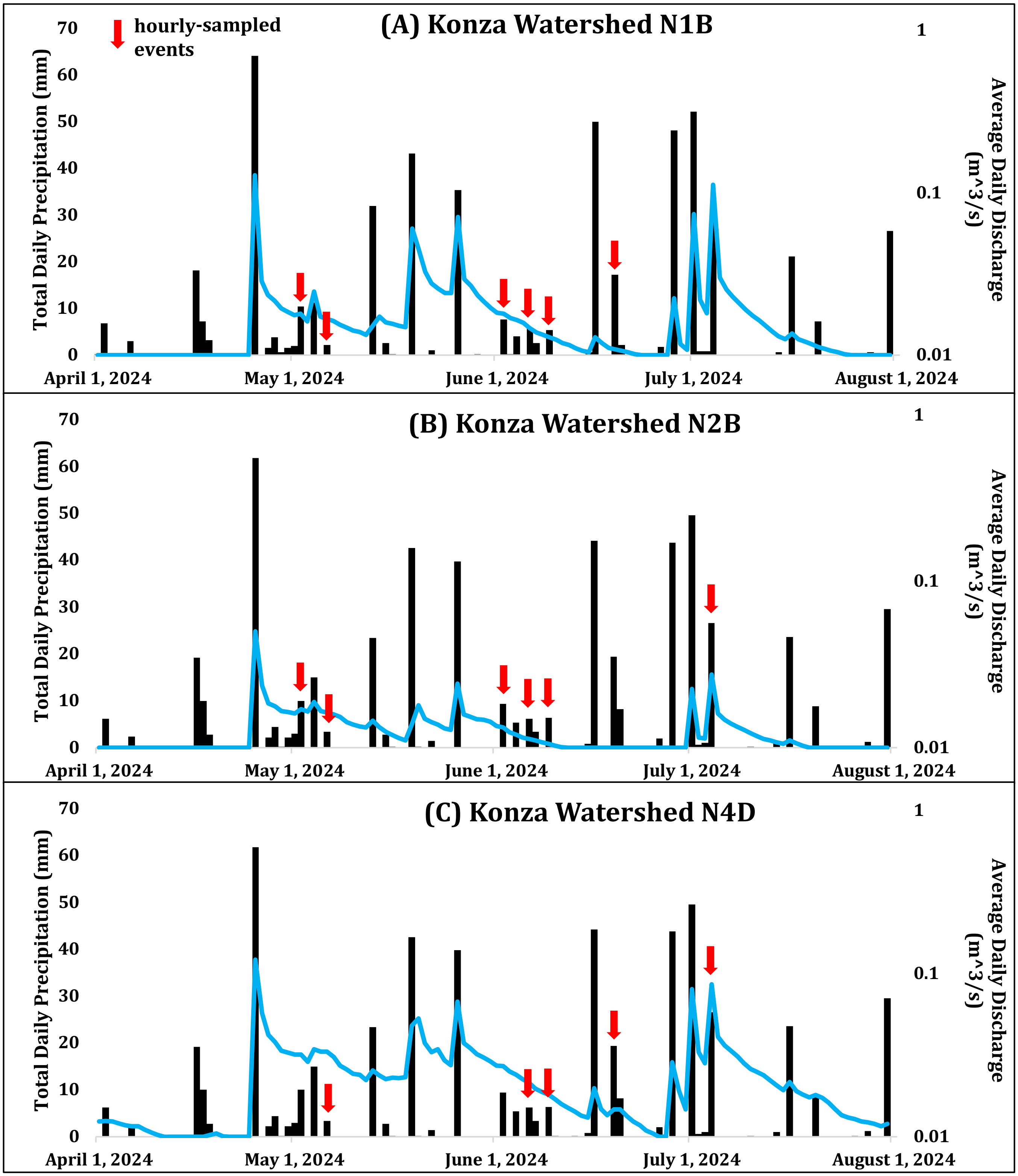

Figure 6. Total daily precipitation (black bars), average daily discharge (blue line), and hourly samples rainstorms (red arrows) for each watershed (A) N1B, (B) N2B, and (C) N4D. *0.01 was added to each discharge to display no flow days on log scale.

The rainstorms selected for hourly stream sampling represented a range of conditions with precipitation event size ranging from 2.2 mm to 30.0 mm (***Fig. 6***). Streamflow prior to each event varied over the study period for each watershed. Moreover, storms earlier in the study period occurred under cooler conditions with lower potential for evaporation compared to those later in the summer.

The results of our 2024 ΔQ/P/A calculations are summarized in ***Figure 7***, where we observe that the least encroached watershed (N1B) experiences larger changes in discharge than the less encroached watersheds (N2B & N4D) given equal amounts of precipitation. We also observed that the intermediately encroached watershed (N2B) experiences the smallest change in discharge during rainstorms. Additionally, mean 2024 ΔQ/P/A on the least encraoched watershed (N1B) was higher than the more encroached watersheds (N2B & N4D) (2.08E-05, 1.91E-06, and 4.54E-06 respectivley).

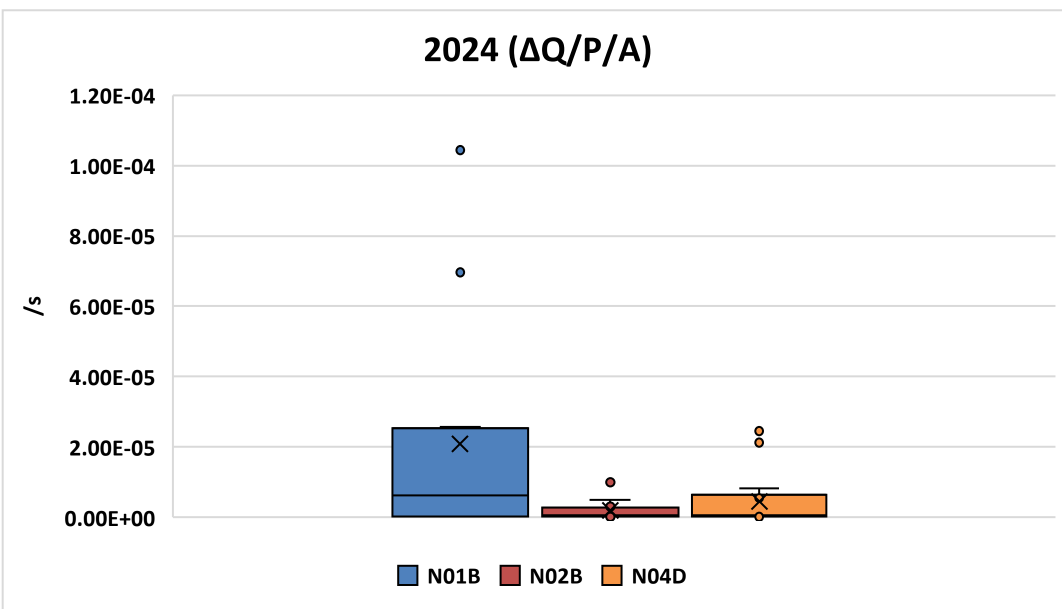

Figure 7. *Box plots for the change in discharge (peak discharge – antecedent discharge) divided by the amount of precipitation (normalized to watershed area) received for all hourly sampled events and events greater than 10mm during our study period for watersheds N1B, N2B, and N4D.*

Our historical analysis revealed that stream discharge response to each storm was, on average, greater for all three watersheds during 2020-2023 compared to 1987-1990 (***Fig. 8***). The difference was the greatest in the least encraoched watershed (N1B) and smallest for the intermediately encroached watershed (N2B). *p* values for the earlier years (1987-1990) are higher than the *p* values for the more recent years (2020-2023) (***Table 4***).

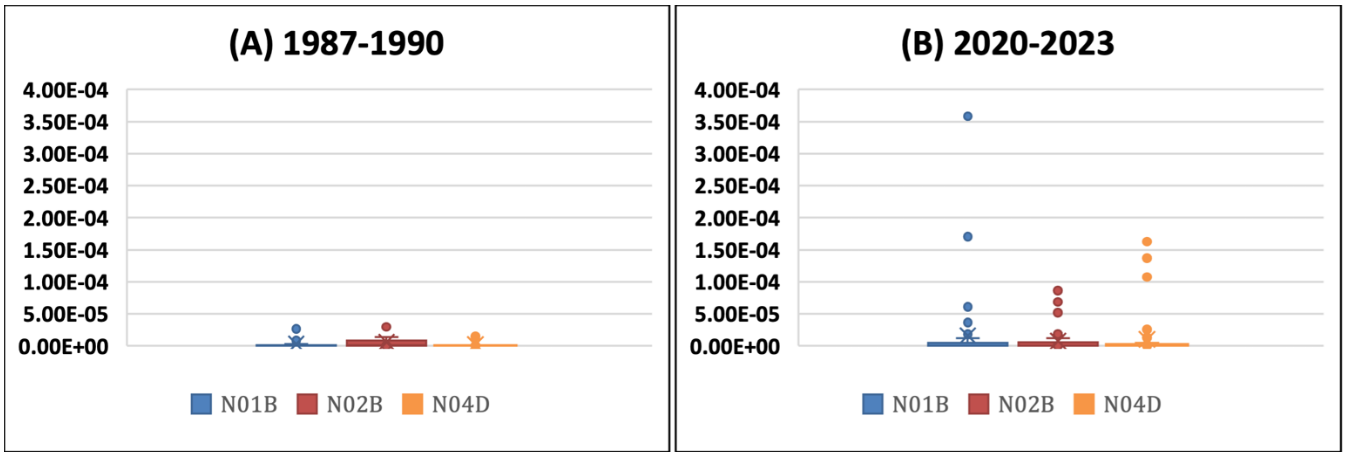

Figure 8. *Box plots displaying the ΔQ/P/A analysis on all three watersheds (N01B blue, N02B red, N04D orange) during the years 1987-1990 (A) and 2020-2023 (B).*

Table 4. *Mean, median, standard deviation (St. Dev.), number of storms (n), and p values for ΔQ/P/A analysis for years 1987-1990 and 2020-2023.*

		N01B	N02B	N04D
1987-1990	Mean	3.11E-06	5.88E-06	2.24E-06
	Median	2.03E-07	1.41E-06	4.17E-07
	St. Dev.	6.69E-06	8.49E-06	4.81E-06
	n	22	13	31
2020-2023	Mean	1.60E-05	7.50E-06	1.04E-05
	Median	4.05E-07	5.57E-07	7.84E-07
	St. Dev.	5.42E-05	1.84E-05	3.03E-05
	n	54	42	60
p **1987-1990 vs 2020-2023**		2.71E-01	7.61E-01	1.42E-01

4.2 Water Chemistry

Figure 9 summarizes the chemical characteristics and major ion concentrations for all 286 stream samples collected within the study. The concentrations of NO_2^-, NO_3^-, Br^-, NH_4^+, TN, and NPOC frequently fell below instrumentation detection limits and are thus excluded from further analysis, however, the full data are provided in Appendix A.

Ca^{2+}, Mg^{2+}, and alkalinity are products of carbonate mineral weathering and were present in all stream water samples. Ca^{2+} concentrations were on average lower in watersheds that were more encroached, mean Ca^{2+} content was 90.84, 88.61, and 71.36 mg/L in N1B, N2B, and N4D respectively (***Fig. 9I***). Ca^{2+} was significantly (p = 1.95E-01 for N1B vs N2B, 1.85E-20 for N1B vs N4D, and 1.88E-12 for N2B vs N4D) lower on the most encroached watershed (N4D) than the less encroached watersheds (N1B and N2B). Mg^{2+} does not vary significantly with the most encroached watershed (N4D) and the least encroached watershed (N1B), but does with the intermediately encroached watershed (N2B) and the other two watersheds, mean content was 16.44, 15.05, and 16.79 mg/L in N1B, N2B, and N4D respectively (p = 2.94E-10 for N1B vs N2B, 1.92E-01 for N1B vs N4D, and 5.83E-07 for N2B vs N4D) (***Fig. 9H***). Alkalinity concentrations were on average lower in watersheds that were more encroached (***Fig. 9A***). Mean alkalinity content was 5.54, 5.34, and 4.80 meq/L in N1B, N2B, and N4D, respectively, but was not significantly different (p = 1.53E-02 for N1B vs N2B, 4.73E-16 for N1B vs N4D, and 5.44E-07 for N2B vs N4D).

pH was on average greater (more basic) in watersheds that are more encroached, although pH differences vary as the streams dry and then wet again (***Fig. 10***). Before drying, mean pH for the hourly sampled events was 7.55, 7.68, and 7.86 in N1B, N2B, and N4D respectively (***Fig. 9B***). pH varied significantly on the most encroached watershed (N4D) then the less encroached watersheds (N1B and N2B) (p = 2.90E-01for N1B vs N2B, 3.18E-16 for N1B vs N4D, and

2.39E-33 for N2B vs N4D). Additionally, mean surface water temperature during the entire study period for N1B, N2B, and N4D was similar, with N4D being slightly higher than the other watersheds (17.05ºC, 17.06ºC, and 17.75ºC, respectively) (p = 3.46E-01 for N1B vs N2B, 2.32E-06 for N1B vs N4D, and 2.27E-05 for N2B vs N4D).

SO_4^{2-} and Sr^{2+} concentrations were significantly higher in the less encroached watershed, average for the most encroached watershed, and least in the intermediately encroached watershed. Mean SO_4^{2-} content was 21.65, 18.05, and 18.73 mg/L in N1B, N2B, and N4D, respectively (p = 1.08E-14 for N1B vs N2B, 1.12E-06 for N1B vs N4D, and 2.62E-01 for N2B vs N4D) (***Fig. 9E***). Mean Sr^{2+} concentrations were 4.14, 3.51, and 3.63 mg/L in N1B, N2B, and N4D, respectively (p = 5.95E-10 for N1B vs N2B, 1.12E-08 for N1B vs N4D, and 2.21E-01 for N2B vs N4D) (***Fig. 9J***).

F^-, Na^+, and Cl^- concentrations varied little across watersheds. Mean F^- concentrations were 0.42, 0.37, and 0.40 mg/L in N1B, N2B, and N4D, respectively (p = 2.47E-23 for N1B vs N2B, 3.81E-03 for N1B vs N4D, and 8.71E-07 for N2B vs N4D) (***Fig. 9C***). Mean Na^+ concentrations were 4.78, 3.61, and 4.00 mg/L in N1B, N2B, and N4D, respectively (p = 1.56E-30 for N1B vs N2B, 4.71E-14 for N1B vs N4D, and 2.88E-04 for N2B vs N4D) (***Fig. 9F***). Chlorine (Cl_-) concentrations were on average higher in the least encroached watersheds, with concentrations of 2.71, 2.35, and 1.97 mg/L in N1B, N2B, and N4D, respectively (p = 2.67E-06 for N1B vs N2B, 1.66E-16 for N1B vs N4D, and 4.29E-06 for N2B vs N4D) (***Fig. 9D***).

K^+ was not significantly different with encroachment, with mean concentrations being relatively similar, 0.97, 1.04, and 1.04 mg/L in N1B, N2B, and N4D, respectively (p = 1.22E-01for N1B vs N2B, 2.38E-01 for N1B vs N4D, and 9.52E-01 for N2B vs N4D) (***Fig. 9G***).

The mean, median, standard deviation, and calculated p values for all measured solutes can be found in Appendix C.

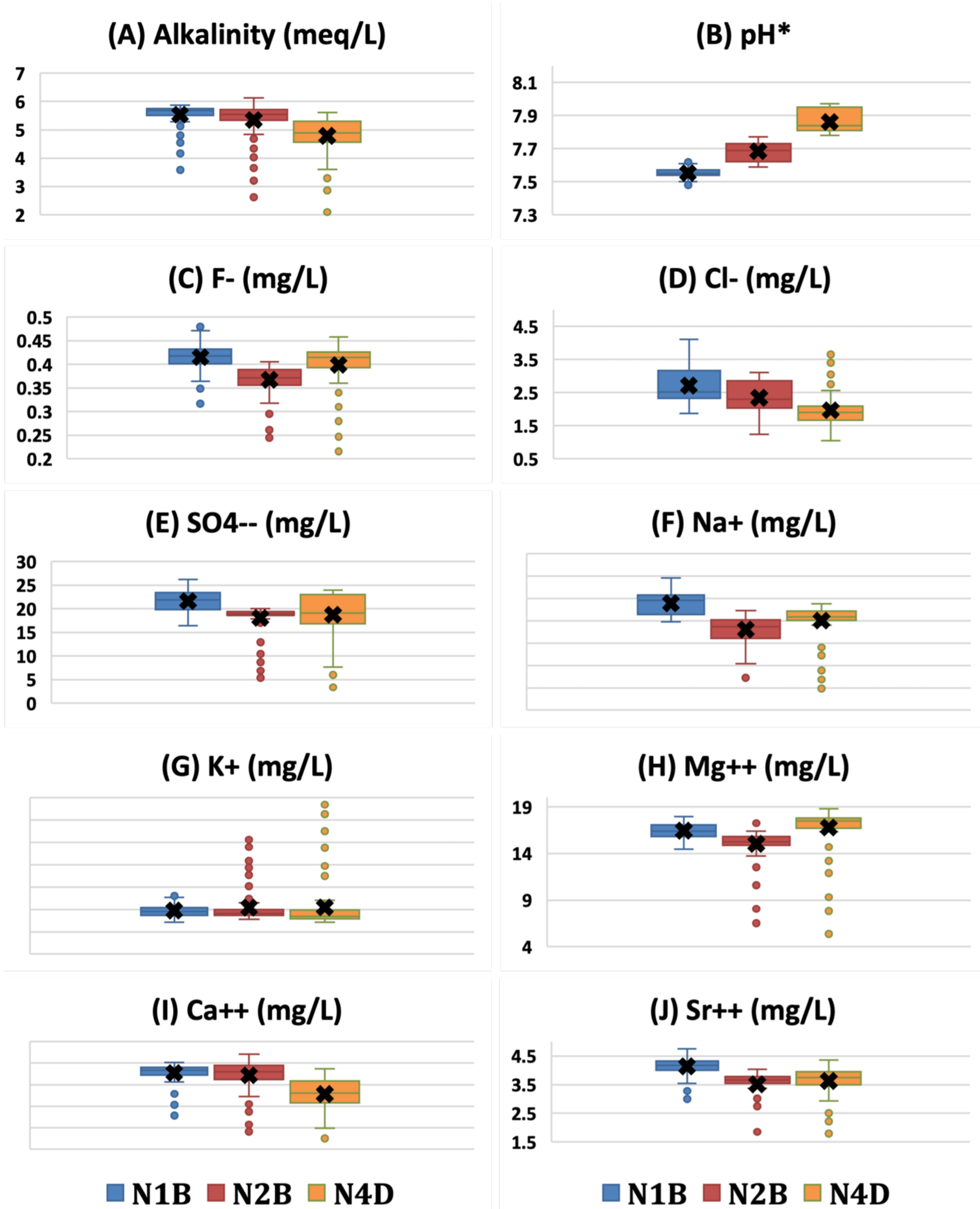

Figure 9. *Box plots for alkalinity (A), pH* (B), fluoride (C), chloride (D), sulfate (E), sodium (F), potassium (K), magnesium (H), calcium (I), and strontium (J) concentrations for all surface water samples collected during the study period across all three watersheds. X marks the mean concentrations and dots mark outliers. *pH for events 1-5 only.*

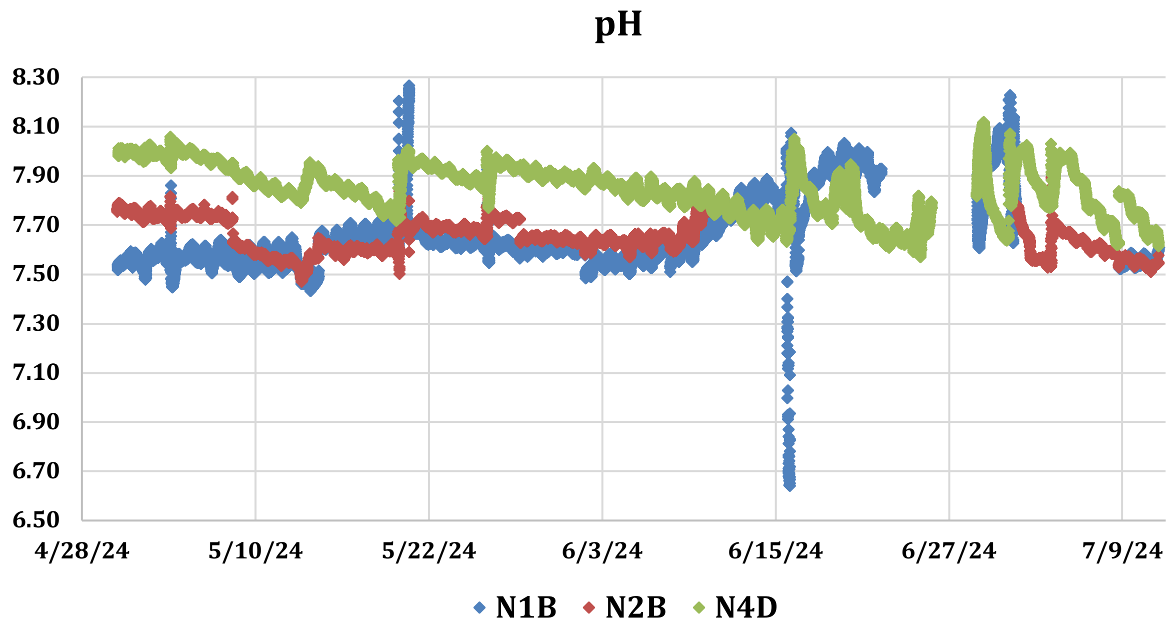

Figure 10*. pH measured across all three watersheds every 5 minutes while flow was active. Gaps in data represent times when flow was not active or when instruments were not recording.*

4.3 Concentration-Discharge Behavior

We calculated the *b* parameter and the CVc/CVq for each solute measured during the entire sampling period, across all three watersheds (***Fig. 11***). Solutes on the least encroached watershed (N1B) tend to be more chemodynamic than those same solutes found on the more encroached watersheds. The CVc/CVq value for Cl^- in N1B is nearly three times that of N2B and N4D (0.29, 0.12, and 0.14, respectively). The CVc/CVq value for Ca^{2+} in watershed N1B is approximately double that of N2B and N4D (0.20, 0.09, and 0.11, respectively. Additionally, Cl^- and Ca^{2+} were two of only three solutes with positive b parameter values in N1B but negative b parameter values in the more encroached watersheds. These results are consistent with dilution behavior in the more encroached watersheds but mobilization behavior in less encroached watersheds. Similarly to Cl^- and Ca^{2+}, the CVc/CVq value for SO_4^{2-} in watershed N1B is also nearly twice that of N2B and N4D (0.19, 0.09, and 0.13 respectively).

Potassium however follows a different trend, whereas the CVc/CVq values for the least encroached watersheds N1B and N2B are slightly less than those of the most encroached watershed (0.21, 0.22, and 0.28 respectively). The b parameter for K^+ is negative, consistent with dilution, in the less encroached watershed (N1B), and positive, consistent with enrichment, in the more encroached watersheds (N2B and N4D). Magnesium CVc/CVq values varied little with encroachment and were identical at N1B, N2B, and N4D (0.07, 0.07, and 0.07 respectively). The b parameter of magnesium did however change slightly at N1B, N2B, and N4D (-0.04, -0.09, and -0.14), consistent with a stronger dilution behavior occurring with increasing encroachment.

Fluoride displayed higher CVc/CVq values on the least encroached watershed (N1B) than the two encroached watersheds N2B and N4D (0.14, 0.05, and 0.06 respectively) and the b parameter remained similar within the three watersheds. Similarly, sodium also showed slightly higher CVc/CVq values on N1B than N2B or N4D (0.15, 0.10, and 0.09 respectively). Strontium CVc/CVq values were 0.20, 0.08, and 0.07 at N1B, N2B, and N4D respectively.

Lastly, alkalinity displayed a much more chemodynamic behavior at the least encroached watershed (N1B) and was similarly chemostatic at the encroached watersheds (N2B and N4D) (0.15, 0.07, and 0.07 respectively). Alkalinity was the third solute to have a positive b parameter (0.04) on the most encroached watershed (N1B) and negative b parameters on the more encroached watersheds (-0.02 at N2B & -0.04 at N4D). Thus, the result is consistent that alkalinity displays a flushing behavior at the least encroached site (N1B) and a dilution behavior at the more encroached sites (N2B and N4D).

Ur, Sr, and Ba had negative b values, consistent with diluting behavior. and the CVc/CVq values for those trace elements varied little across watersheds N2B and N4D (0.29, 0.24, 0.23 and 0.37, 0.33, 0.20, respectively).

Ar and B CVc/CVq varied little across the two watersheds and were near chemostatic behavior. The CVc/CVq values for Ar at N2B and N4D were 0.23 and 0.24 respectively and the CVc/CVq value for boron at N2B and N4D was 0.08 and 0.10 respectively. The CVc/CVq value for Cu was consistent with enriching behavior and nearly identical for N2B and N4D (0.90 and 0.91 respectively).

The CVc/CVq for Mn, Rb and Fe was consistent with chemodynamic behavior in N2B but strong enriching behavior in N4D. The CVc/CVq values for Mn, Rb, and Fe at N2B and N4D were 0.40, 0.16, 0.28 and 1.30, 0.46, 0.66, respectively. La and P results were consistent with enriching behavior at N2B and N4D but both elements were much more chemodynamic in N4D compared to N2B. The CVc/CVq value for La and P in N4D (1.57 and 1.85, respectively) was nearly twice that for N2B (0.81 and 1.05, respectively).

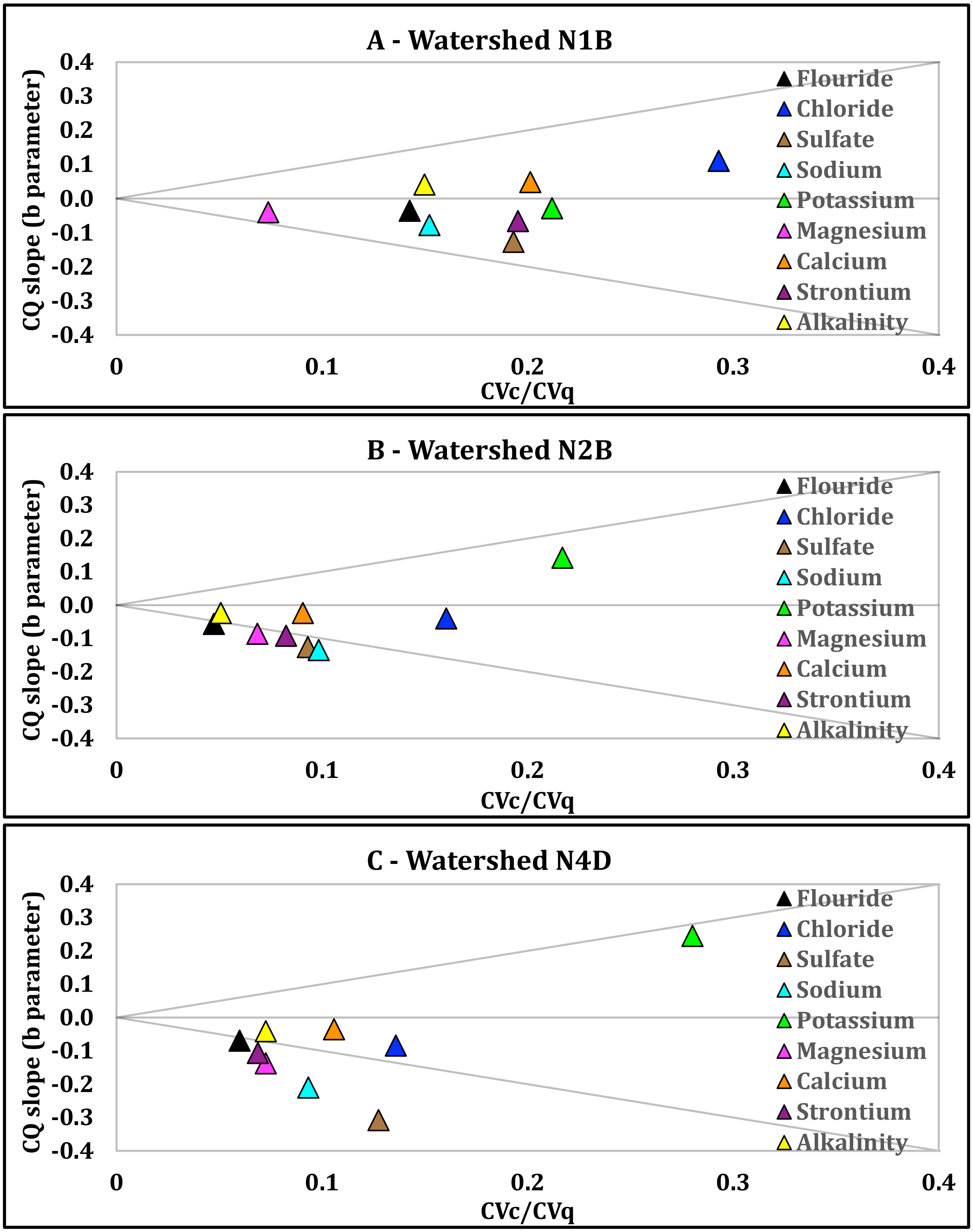

Figure 11. *b parameter vs. CVc/CVq plots for all surface water samples collected at N1B (A), N2B (B), and N4D (C).*

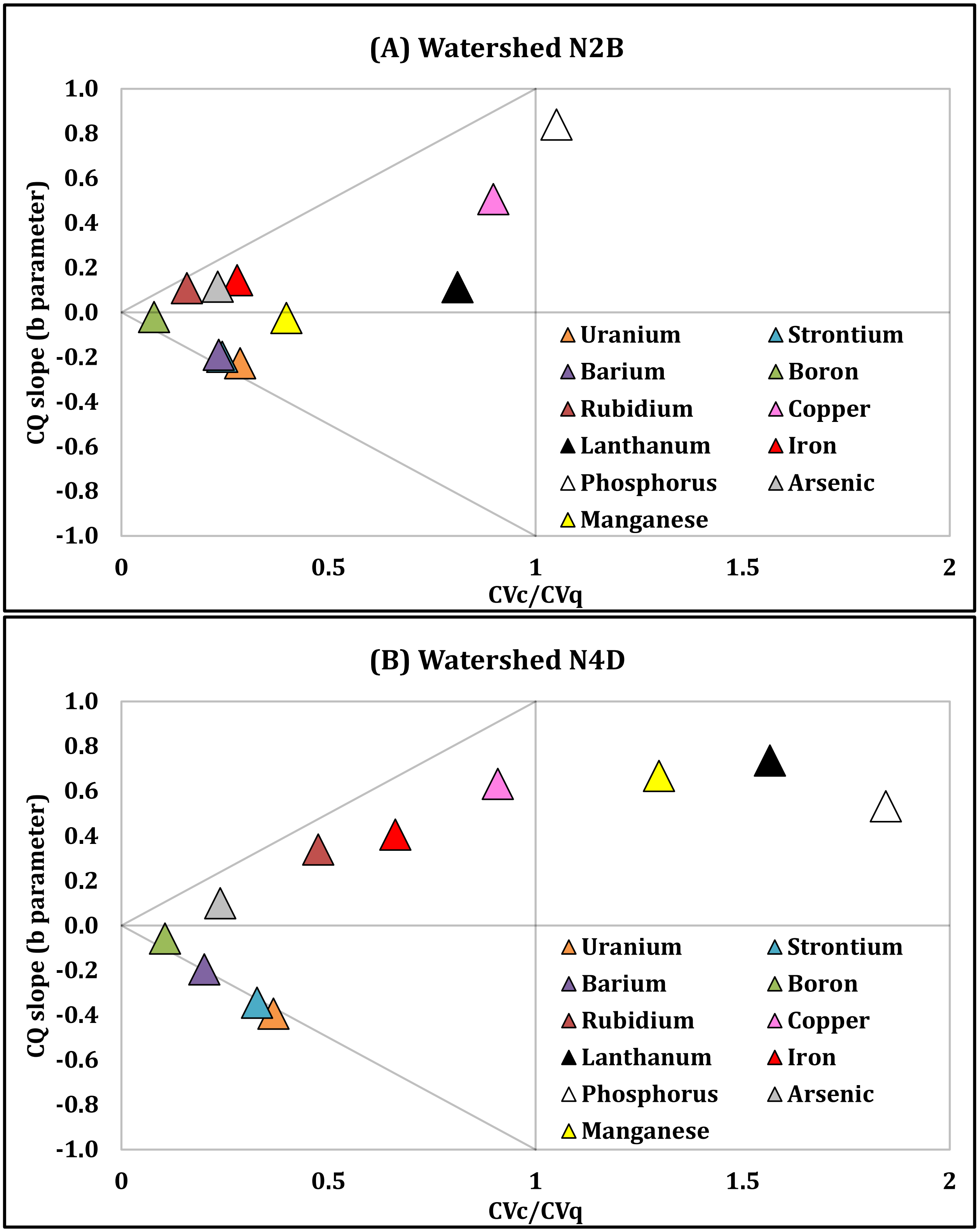

Figure 12. *CQ slope (b parameter) vs. CVc/CVq plots for trace elements for event seven only at N2B (A) and N4D (B).*

4.4 Stable Water Isotopes

Stable water isotopes ($\delta^{18}O$ and δD) were analyzed for all 252 stream samples and 16 precipitation samples collected during the study (***Fig. 13A***). The Global Meteoric Water Line (GMWL) is plotted against our collected samples to ensure accuracy and is defined by the line $\delta D = 8*\delta^{18}O + 10$ (Craig, 1961). Previous research at Konza Prairie N4D watershed determined a Local Meteoric Water Line (LMWL) defined as $\delta D = 7.4*\delta^{18}O + 2.4$ (Hatley et al., 2023). Precipitation samples collected during event five were determined to be outliers and are not included in regression calculations or further analysis (***Fig. 13F***). The linear regression line that fits the data collected during this study is defined by the line $\delta D = 6.9*\delta^{18}O + 4.0$ with $R^2 = 0.96$.

Stream water $\delta^{18}O$ values ranged between -6.1‰ and -4.8‰ with little variation between watersheds N1B, N2B, and N4D (-6.1‰ and -5.5‰, -6‰ and -5.2‰, -6‰ and -4.8‰, respectively). Precipitation $\delta^{18}O$ values ranged between -5.8‰ and 0.5‰, and also varied little between watersheds N1B, N2B, and N4D (-5.7‰ and -0.7‰, -5.8‰ and 0.5‰, -5.8‰ and -0.6‰, respectively). The precipitation and stream water $\delta^{18}O$ values measured for event six (***Fig. 13G***) were not isotopically distinct. The $\delta^{18}O$ values ranged from-5.7‰ to -5.6‰ and from -5.7‰ to -5.4‰ for precipitation and stream water, respectively. Given the overlap, the results for storm six were excluded from the hydrograph separation analysis. Precipitation and stream water $\delta^{18}O$ ranges for event one (***Fig. 13B***), event two (***Fig. 13C***), event three (***Fig. 13D***), event four (***Fig. 13E***), and event seven (***Fig. 13H***) were found to be isotopically distinct, making them good candidates for hydrograph separation analysis.

Stream water δD values ranged between -37‰ and -25‰ with little variation between watersheds N1B, N2B, and N4D (-37‰ and -33‰, -37‰ and -28‰, -37‰ and -25‰, respectively). Precipitation δD values ranged more, between -52‰ and 10‰, and also varied little between watersheds N1B, N2B, and N4D (-44‰ and -3‰, -51‰ and 10‰, -52‰ and 2‰, respectively). The δD values for event six (***Fig. 13G***) ranged from -37‰ to -36‰ and from -35‰ to -33‰ for precipitation and stream water, respectively. Given the overlap, the results for storm six were excluded from the hydrograph separation analysis. Precipitation and stream water δD ranges for event one (***Fig. 13B***), event two (***Fig. 13C***), event three (***Fig. 13D***), event four (***Fig. 13E***), and event seven (***Fig. 13H***) were found to be isotopically distinct, making them good candidates for hydrograph separation analysis.

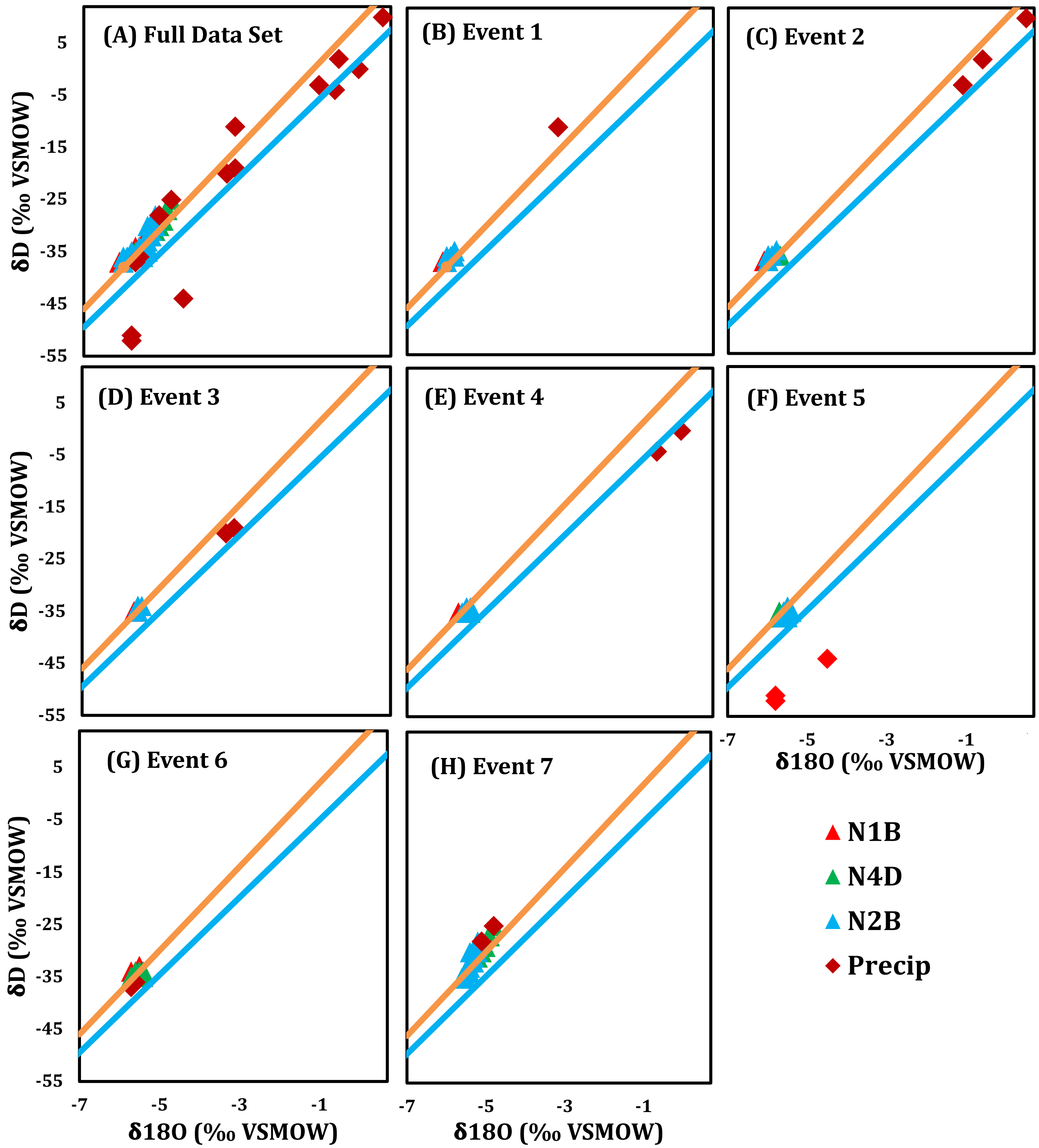

Figure 13. *Stable water isotopes in all surface water and precipitation samples collected during the study. The solid orange line indicates the Global Meteoric Water Line (GMWL) and the solid blue line indicates the Local Meteoric Water Line (LMWL). Graphs displaying data for (A) all samples collected, (B) samples in event one, (C) event two, (D) event three, (E) event four, (F) event five, (G) event six, and (H) event seven.*

4.5 Isotope Hydrograph Separation

The fractional contribution of event water (direct precipitation and runoff) for each sampled precipitation event was determined using the average of two end-member calculations with $\delta^{18}O$ and δD as tracers (***Fig. 14***). Stream water samples collected before precipitation started were used as pre-event $\delta^{18}O$ and δD values whereas precipitation isotope rates were used as the event $\delta^{18}O$ and δD values. The end-member compositions are summarized in **Table 5**.

The fraction of event water for event one (***Fig. 14A***) peaked at 9.02% for the least encroached watershed (N1B) and 7.42% for the intermediately encroached watershed (N2B). No sample was taken from the most encroached watershed (N4D) during this event due to equipment complications. Peak event water fractions for event two (***Fig. 14B***) were similar for N1B, N2B, and N4D (3.47%, 3.67%, and 4.06%, respectively). Event three (***Fig. 14C***) peak event water fraction was slightly lower for watersheds N1B compared to N2B (3.12% and 5.61%, respectively). Peak event water fractions for event four (***Fig. 14D***) were similar for N1B and N4D (1.00% and 1.04%, respectively, and highest for N2B (3.25%).. Event four results indicated negative event fraction values (down to -1.04%) for the most encroached watershed (N4D), potentially due to a start time error which resulted in the first samples being taken while light sprinkling was occurring. Event seven (***Fig. 14G***) peak event water fractions for watersheds N2B and N4D were far higher than the other sampled events (up to 90.00% and 100.00%, respectively), with the most encroached watershed (N4D) including the most event water. Fractions for event water and pre-event water for all samples are included with the water chemistry data in Appendix A.

Table 5. *Stable water isotope values used for end-member mixing calculations for event water and pre-event water. All isotopic values are in ‰ VSMOW.*

Event	**Date**	**Watershed**	**Event End-Member**		**Pre-event End-Member**	
			$\delta^{18}O$	**δD**	**$\delta^{18}O$**	**δD**
one	05/01-05/02	N1B	-3.2	-11	-6.1	-37
		N2B	-3.2	-11	-6	-37
two	05/06-05/07	N1B	-1.1	-3	-6.1	-37
		N2B	0.5	10	-6	-37
		N4D	-0.6	2	-6	-37
three	06/02	N1B	-3.2	-19	-5.6	-35
		N2B	-3.4	-20	-5.6	-35
four	06/07-06/08	N1B	-0.7	-4	-5.7	-35
		N2B	-0.1	0	-5.6	-35
		N4D	-0.7	-4	-5.5	-35
five	06/08-06/09	N1B	-4.5	-44	-5.6	-35
		N2B	-5.8	-51	-5.5	-35
		N4D	-5.8	-52	-5.5	-35
six	06/18-06/19	N1B	-5.7	-37	-5.5	-34
		N4D	-5.6	-36	-5.4	-34
seven	07/03-07/04	N2B	-5.1	-28	-5.6	-35
		N4D	-4.8	-25	-5.6	-35

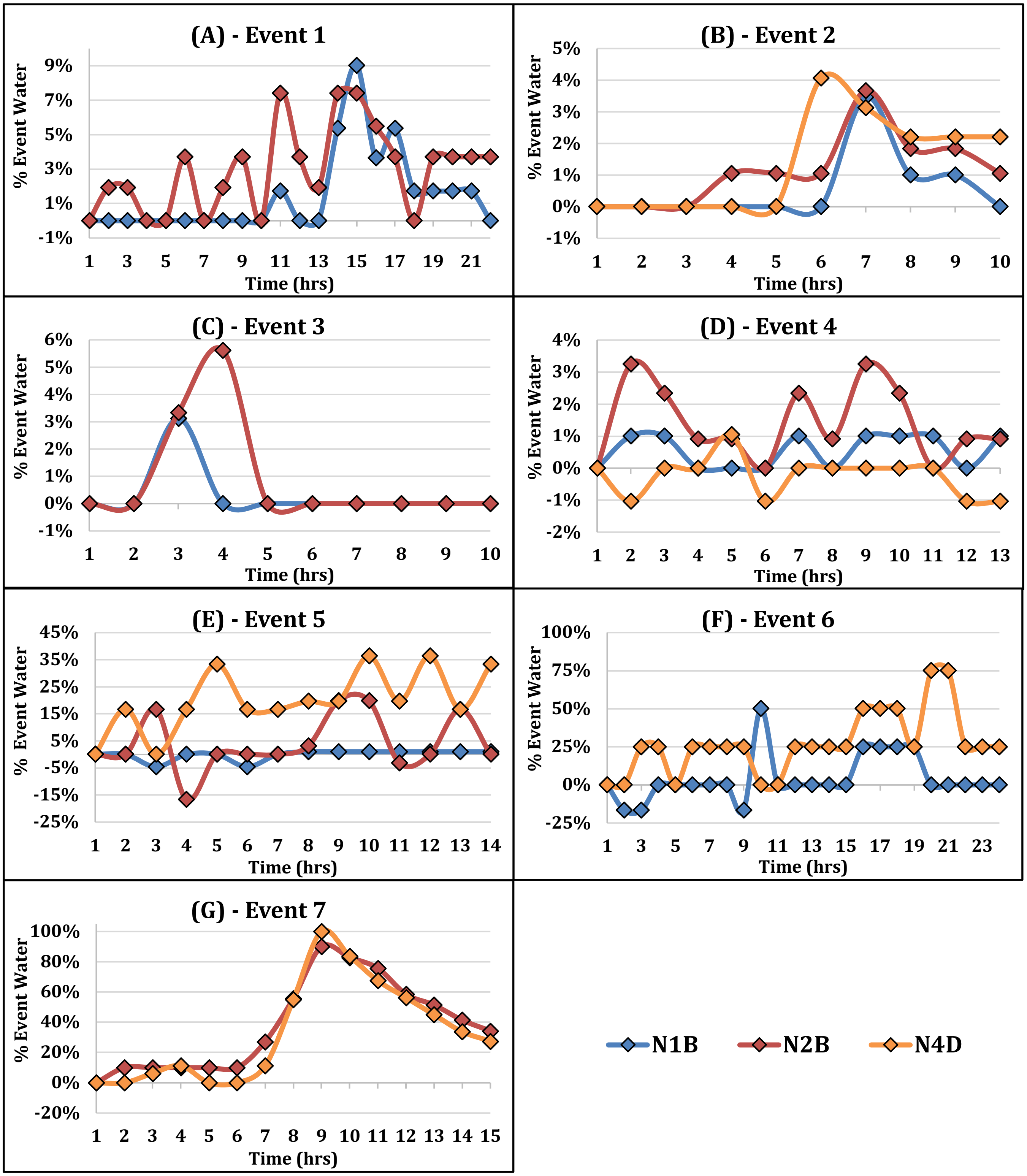

Figure 14. *Percentage of event water vs. time for (A) event one, (B) event two, (C) event three, (D) event four, (E) event five, (F) event six, and (G) event seven.*

The fractional contribution of event water increases during storms, however antecedent hydrologic conditions can influence the magnitude of the increase. Hydrologic characteristics such as the maximum fraction of event water (fQ_e), maximum flow rate of event water during the event ($Q_e = fQ_e*Q_{stream}$), the amount of precipitation (P), the antecedent stream discharge (aQ), and the maximum change in discharge (dQ) are all needed to best understand the behaviors of these watersheds.

The largest fQ_e values occur during event seven, which immediately followed a period where all three streams dried and were re-wetted from two large rainstorms (46 mm and 51.2 mm respectively) occurring on 06/28 and 07/01 (***Fig. 6)*.** Event one received similar amounts of precipitation at N1B and N2B (10.4 mm and 10.0 mm, respectively) and equated to a slightly higher fQ_e at N1B than N2B (0.0902 and 0.0742, respectively).

Event two received a very small amount of precipitation across N1B, N2B and N4D (2.2 mm, 3.4 mm, and 3.4 mm, respectively) and resulted in the lowest fQ_e value on N1B, a mid-range on N2B, and the highest on N4D (0.0347, 0.0367, and 0.0406, respectively). We see this trend continue during event three where N1B and N2B received again small amounts of precipitation (7.6 mm and 9.4 mm, respectively) which resulted in fQ_e values of 0.0312 and 0.0561 at N1B and N2B respectively. The larger fQ_e values on the more encroached watersheds could be resulting from differences in precipitation amounts, where the less encroached watershed (N1B) received 35% less precipitation than the more encroached watersheds during event two and 19% less precipitation during event three.

Event four also received a small amount of precipitation across N1B, N2B, and N4D (5.8 mm, 6.2 mm, and 6.2 mm, respectively), and occurred during a time when antecedent discharge across the watersheds was relatively low (0.005, 0.001, and 0.010 m^3/s respectively). These low flow conditions resulted in an fQ_e values that varied substantially (***Fig. 14D***) across the watersheds N1B, N2B, and N4D (0.010, 0.0312, and 0.0104 respectively).

Table 6*. Hydrologic characteristics for hourly sampled events analyzed for isotope hydrograph separation. fQ_e is the maximum fraction of event water during the storm, Q_e is the maximum discharge of event water during each storm, P is the amount of precipitation received, aQ is the antecedent discharge, and dQ is the maximum change in discharge during the event*

Event	**Date**	**Watershed**	**fQ_e**	**Q_e (m^3/s)**	**P (mm)**	**aQ (m^3/s)**	**dQ (m^3/s)**
#01	05/01-05/02	N1B	0.09	0.00098	10.4	0.007	0.004
		N2B	0.07	0.00047	10.0	0.006	0.004
#02	05/06-05/07	N1B	0.03	0.00024	2.2	0.007	0.000
		N2B	0.04	0.00024	3.4	0.006	0.001
		N4D	0.04	0.00102	3.4	0.023	0.003
#03	06/02	N1B	0.03	0.00030	7.6	0.008	0.003
		N2B	0.06	0.00027	9.4	0.003	0.002
#04	06/07-06/08	N1B	0.01	0.00004	5.8	0.005	0.001
		N2B	0.03	0.00004	6.2	0.001	0.001
		N4D	0.01	0.00010	6.2	0.010	0.001
#07	07/03-07/04	N2B	0.90	0.03870	26.6	0.001	0.156
		N4D	1.00	0.19235	26.6	0.018	0.763

Chapter 5 - Discussion

The primary goal of this study was to better understand and evaluate the potential impacts of woody encroachment on streamflow generation and chemistry. To accomplish this, we sampled streams in three variably encroached watersheds during seven storm events during the 2024 growing season and applied isotope hydrograph separation, C-Q calculations, and $\Delta Q/P$ analysis to the results. Below we discuss the results of these analyses, and the potential impacts woody encroachment has on streamflow sources and chemistry.

5.1 Stream water sources

Precipitation samples taken during events one (***Fig. 13B***), two (***Fig. 13C***), three (***Fig. 13D***), four (***Fig. 13E*)**, and seven (***Fig. 13H***) were all isotopically distinct from the stable water isotope values of the stream water, making all five of the event's good candidates for isotope hydrograph separation analysis (***Fig. 14***). However, isotope compositions for storms five (***Fig. 12F***) and six (***Fig. 12G***) were inconsistent with the needs of the analysis and thus excluded. Precipitation samples from event five had low δD values compared to other precipitation samples collected during the study. Potential explanations for the low values include sub-cloud evaporation or continental convection. Sub-cloud evaporation is the evaporation of rain droplets as they fall from the cloud base to the ground, which is a common occurrence in the Midwest (Zhu et al., 2021). However, this is unlikely given that the precipitation occurred during a thunderstorm and near saturation conditions. Continental convection is the rise of warm, moist air over land under high relative humidity, which reduces the fractionation of rainwater and can lead to low d-excess values (D. Wang et al., 2023). Consistent with this process, precipitation isotope values from event five fall along a line parallel but separate from the local meteoric water line (LMWL). Event six precipitation isotope ratios (***Fig. 13G***) aligned with the LMWL but were not isotopically distinct from the corresponding stream samples, making them useless as event tracers.

Our isotope hydrograph separation analysis indicate that event water contributed a slightly higher fraction of streamflow in more encroached watersheds than in less encroached watersheds during events two, three, and seven. These observations contradict the conclusions of (Qiao et al., 2017; Sullivan et al., 2019) who found that woody plant encroachment reduces runoff generation and encourages deep vertical interflows. One potential reason for the differences observed between our study and others may be contributed by the small intensity of the rainstorms that we sampled (***Table 6***). Previous studies using isotope hydrograph separation to determine streamflow sources have argued that event intensity directly controls the fractionation of event water and pre-event water, with variation between environments (Klaus & McDonnell, 2013). Furthermore, low intensity rainstorms could be quickly infiltrating the subsurface, applying pressure onto the existing water table and aquifers, therefore flushing more water into the streams via springs and riparian seeps. This process could be further accelerated on the most encroached watershed (N4D) due to the increased soil permeability and porosity caused be woody plant encroachment (Jarecke et al., 2025; Sullivan, Stops, et al., 2019a).

Runoff generation is limited at Konza Prairie because of the large soil macropores and bedrock fractures that are common throughout the landscape (Macpherson et al., 2008; Tsypin & Macpherson, 2012), therefore all of our analyzed rainstorms fell below 10% event water contribution except for event seven (***Fig. 14G***). That event not only had the largest amount of precipitation of the storms sampled hourly, but it also occurred within two weeks of two relatively large storms. Increased soil moisture from those antecedent storms would work to decrease the infiltration capacity of watershed soils (Horton, 1933), making it easier to generate runoff. We suggest that analysis of large rainstorms (>10-15 mm) is needed to compare encroachments impacts on runoff generation using hydrograph separation analysis.

Although runoff generation tended be slightly higher in the more encroached watershed, our ΔQ/P/A analysis results for the most recent years (2020-2024) indicate that streamflow in the least encroached watershed (N1B) was the most responsive to each storm event (***Fig. 7 & 8***). Previous studies have concluded that grass covered land retains near-surface soil water better than shrub covered areas given identical precipitation amounts, which in turn leads to encroachment drying soils and increasing infiltration potential (Jarecke et al., 2025), potentially amplified by encroachments elevated evapotranspiration rates. Soil drying due to woody plant encroachment could be one key driver to the differences we observe in our ΔQ/P/A analysis.

However, if this model matched ours perfectly, we would expect to observe the most encroached watershed (N4D) would have the lowest ΔQ/P/A results, which is not what we observe (***Fig. 7***). We think that the intermediately encroached watershed (N2B) being the least responsive to storm events may be attributed to the fact that the watershed has been previously altered. Dodds et al., (2023) began experimental cutting of all above ground woody plant species (trees and shrubs) within 30 m of the headwater stream running through watershed N2B. They continued this investigation by cutting half of all above ground riparian zone woody species every other year, alternating between years for ten years before concluding the project in 2020. This method, although effective at initially removing above ground woody plant vegetation, leaves the underground root systems intact and potentially creates legacy pathways for groundwater infiltration. Previous woody plant removal studies within grassland systems have showed mixed results with some increasing streamflow and groundwater discharge (Bosch &

Hewlett, 1982), with others not observing similar trends (Dugas & Hicks, n.d.; Wilcox, 2002; Wilcox et al., 2006). Dodds et al., (2023) argued that the removal of the above ground riparian woody plant species at N2B did not dramatically increase infiltration within the watershed and will likely have legacy effects lasting for years or decades. After the research team's initial large-scale removal of riparian tree coverage on N2B they also observed an immediate sizeable increase in riparian shrub species growth. The rapid expansion of shrub species within the riparian zone on N2B overall decreased the amount of water making it into the stream, even after a decade of woody plant removal (Dodds et al., 2023).

Additionally, climate change is making storm events more intense (Dore, 2005; Marvel et al., 2023), which may be why we observe watersheds being more responsive to storm events on all three watersheds in the most recent years (2020-2024) as compared to years further in the past (1987-1990). Moreover, Konza Prairie has been observed becoming progressively wetter and warmer over the past couple of decades while simultaneously decreasing streamflow discharge (Sadayappan et al., 2023). We observe that streams have become more responsive over time with an increased storm intensity (***Fig 8***); however, encroachment may be affecting the extent of the stream responsiveness. Since encroachment is increasing soil permeability (Jarecke et al., 2025; Keen et al., 2023; Sullivan, Stops, et al., 2019) and thereby funneling more water belowground, increased stream responsiveness due to climate change could be lessened by encroachment. The large increase in responsiveness on the least encroached watershed (N1B) and the smaller increase in intermediately encroached watershed (N2B) that we observe supports the idea that woody encroachment may be lessening the effects of climate change on stream responsiveness.

5.2 Sources of solutes to streamflow

Although we see mixed results from our analysis of streamflow sources based on isotope hydrograph separation and our ΔQ/P/A data, variations in the concentrations of stream water solutes with changing discharge (C-Q analysis) is consistent with differences in solute sources between watersheds (***Fig. 11***). Magnesium (Mg^{2+}), calcium (Ca^{2+}), bicarbonate (HCO_3^-), and strontium (Sr^{2+}) are all considered mineral weathering products and are commonly found in significant quantities within the groundwater of our study area. Soil water will collect CO_2 and dissolve minerals like dolomite (1) and calcite (2) while infiltrating the subsurface through the following reactions.

$$CaMg(CO_3)_2 + 2CO_2(aq) + 2H_2O \leftrightarrow Ca^{2+} + Mg^{2+} + 4HCO_3^- \quad (1)$$

$$CaCO_3 + CO_2(aq) + H_2O \leftrightarrow Ca^{2+} + 2HCO_3^- \quad (2)$$

Although strontium is not directly included in these mineral dissolution equations, it is often found within Permian aged limestones like the ones found at Konza Prairie (Brookins et al., 1969). Macpherson et al., (2008) determined that dolomite and high Mg^{2+} calcite are not abundant within bedrock at Konza Prairie and is therefore an unlikely source of Mg^{2+}, they instead suggest that ion exchange sites in surface soils and mudrock layers are the sources of Mg^{2+}. The chemostatic behaviors of Mg^{2+} implies that the solute has a somewhat homogenous distribution throughout the watersheds and that the solutes mobilization may not be affected by encroachments alteration of flow pathways and subsurface water routing (***Fig. 10***).

The more chemodynamic behavior of Ca^{2+}, HCO_3^-, and Sr^{2+} is likely due to their higher concentrations in the groundwater at the less woody encroached watershed (N1B) (***Fig. 9I & 10J***) (Kirk & Macpherson, 2024). Previous studies at Konza Prairie argue that because woody encroachment is creating flow pathways through near-surface soils, soil water residence time is decreased and therefore decreases open-system near surface weathering while increasing closed-system bedrock weathering, which ultimately results in a lower concentration of CO_2 and mineral weathering products in the groundwater (Anhold et al., 2025). Anhold et al., (2025) also argues that as soil water residence time and the proportion of open-system weathering increases, pH decreases. Further supporting evidence that woody encroachment is decreasing open-system weathering can be observed in the clear distinction we see in average pH within our streams (***Fig. 9B***). Moreover, if a greater amount of open-system mineral weathering is occurring in less encroached watersheds, this could potentially create larger stockpiles of these ions in groundwater that may be released during the infiltration of small amounts of precipitation. Increased infiltration (i.e. rainstorms) likely applies additional pressure to existing stockpiles of Ca^{2+}, HCO_3^-, and Sr^{2+} rich waters, flushing those waters out during disturbance events.

Sulfate (SO_4^{2-}) was found in high concentrations across all three watersheds and displayed dilution behavior, however the ion was the most chemostatic in watershed N2B and most chemodynamic in N1B (***Fig. 11***). Compared to groundwater, soil water contains high concentrations of SO_4^{2-} (Tsypin & Macpherson, 2012) which can be mobilized with large amounts of runoff occurring. The concentration and mobilization of SO_4^{2-} directly reflects our ΔQ/P/A observations wherein the least encroached watershed (N1B) is the most responsive to storm events and the intermediately encroached watershed (N2B) is the least responsive due to enhanced subsurface woody root systems. Because the most responsive watershed (N1B) likely receives the highest amount of runoff during rainstorms, an elevated concentration and chemodynamic behavior is observed here.

The chemodynamic behaviors of solutes like Cl^-, and Na^+ in the less encroached watershed (N1B) matches the proposed model of woody encroachment creating deeper flow pathways for subsurface flow because these are ions that are primarily derived from near-surface soils. Previous research at Konza Prairie argued that Cl^- is solely derived from the evapoconcentration of meteoric waters, which would occur near the surface rather than deep within the subsurface (Wood & Macpherson, 2005). Additionally, wildfires have the ability to increase cation concentrations in near-surface soils by exposing them to the atmosphere, while simultaneously producing ash that can later leach into stream water (Swindle et al., 2021). This process is likely why Na^+ concentrations are elevated in the least encroached watershed (N1B), which is burned yearly. The increased residence time model proposed by Anhold et al., (2025) supports our findings of elevated chemodynamic behavior of near-surface solutes in the least encroached watershed (N1B).

Potassium (K^+) displays the opposite behavior, wherein the ion displays a more chemodynamic flushing behavior in more encroached watersheds (N2B and N4D) than in the less encroached watershed (N1B). K^+ can be generated from a multitude of different processes including biotic cycling, the evapoconcentration of meteoric water, or the weathering of illite or atmospheric dust (Macpherson & Sullivan, 2019; Sullivan et al.,). Due to the complex sourcing of K^+, the concentration and mobilization of the ion likely varies throughout different watersheds without a clear connection to woody encroachment.

Previous studies have conducted C-Q analyses on N4D solutes with similar findings as ours. Hatley et al., (2023) and Sullivan et al., (2019) both found geogenic solutes to be mostly chemostatic and SO_4^{2-} to be diluting. While our study and the one completed by Hatley et al., (2023) mainly calculated CVc/CVq values below 0.5, Sullivan et al., (2019) found CVc/CVq values much higher. This difference is likely due to the longer sampling period of Sullivan et al., (2019), which included samples collected from May 2015 through December 2016. The extended sampling period incorporates a broader range of hydrologic conditions, which results in elevated CVc/CVq values. Consistent with this relationship, Swenson et al., (2024) demonstrated that study area stream compositions change as streams dry and become discontinuous .Our study included samples collected only while stream connected and flowing, whereas the data used by Sullivan et al. (2019) spanned times when the stream in N4D was discontinuous.

Aside from the overall differences in CVc/CVq values, one key difference is that Sullivan et al., (2019) found a strong chemodynamic behavior from Mg^{2+}, which may again reflect the extended timescale of their study. Sullivan et al., (2019) argued that variations in flow paths can change throughout the year and cause ions to behave differently depending on conditions. The chemostatic behaviors during the short timescales of our study and Hatley et al., (2023) indicate that Mg^{2+} concentrations are stable during the wet (growing) season. Beyond that, however, results from Sullivan et al. (2019) indicate Mg^{2+} behavior varies.

The trace elements used in C-Q calculations for event seven all displayed high CVc/CVq values (***Fig. 12***), due to the high discharge of the storm and the sizable fraction of event water (***Fig. 14G***). The considerable proportion of event water increased the suspended load of the stream (Pruitt & Kirk, 2025). The elevated chemodynamic behaviors of trace elements on the most encroached site (N4D) suggest that more near-surface soil flow occurred than on the intermediately encroached watershed (N2B), potentially reflecting past alteration of N2B. Because N2B actually has more above ground riparian shrub coverage than N4D, these finding are consistent with (Dodds et al., 2023) research who argued that these riparian woody species are decreasing water inputs into the stream.

5.3 Implications

Ultimately, the models and processes proposed by Anhold et al., (2025), Jarecke et al., (2025), Qiao et al., (2017), Sadayappan et al., (2023), and Sullivan et al., (2019) all work in conjunction to explain how woody plant encroachment is affecting subsurface flow pathways and altering Konza Prairie hydrology. Our analysis builds on these prior studies by investigating changes in streamflow sources and, consequently, the chemistry of the streamflow.

The decreased concentration and mobilization of calcium and strontium, the higher pH, and the lower alkalinity we observed in the encroached watersheds may reflect the changes in soil water residence time and open-system weathering (***Fig. 9, 10, & 11***). As proposed by Anhold et al., (2025), encroachment decreases soil water residence time because woody plants have thicker and deeper roots than grasses that create soil macropores and allow the soil to drain more easily. In turn, this increase in soil permeability decreases the amount of open-system mineral weathering that occurs, which not only decreases the amount of weathering products in the water as it moves belowground, but also the concentration of dissolved CO_2.

These changes have important implications for aquatic habitats and downstream water quality. pH is arguably one of the most important water quality parameters because it has the ability to control the behavior of aqueous processes like acid-base reactions, solubility reactions, and oxidation-reduction reactions (Saalidong et al., 2022). Many aquatic species and microorganisms are reliant on pH consistency to thrive, with most aquatic life preferring pH levels of 6.5-9.0. Additionally, carbonate minerals like calcite are more likely to precipitate at higher pH levels, higher pH equates to higher ratios of CO_3^{2-} in the water which can be combined with existing Ca^{2+} to precipitate calcite. The process described by Anhold et al., (2025) is also decreasing bicarbonate (HCO_3^-) concentrations and mobilization Konza Prairie. Bicarbonate is the primary component of alkalinity in natural waters; therefore, encroachment is lowering the alkalinity of stream water. While pH and alkalinity are closely related, they function differently. Alkalinity refers to the acid neutralizing capacity of water, or simply the ability of water to resist changes in pH. Encroachment potentially decreasing alkalinity (***Fig. 9A***) weakens the system's ability to resist pH changes from process like acid rain, pollution, and other climate disturbances.

Finally, this study directly observes the consequences of the removal of riparian woody plant species on stream flow sourcing and overall chemistry. Dodds et al., (2023) observed that the removal of tree species from the riparian zone can promote woody shrub establishment and expansion, further decreasing the ability of water to enter the stream. We observed a larger decrease in stream responsiveness (***Fig. 7 & 8***) and chemodynamic solute behaviors (***Fig. 11 & 12***) in the intermediately encroached watershed (N2B) than in the most encroached watershed (N4D). We largely attribute these observations to the legacy root systems of the removed riparian vegetation, which work in conjunction with the newly established woody shrub root systems to amplify the effects of encroachment.

5.4 Limitations and future steps

One limitation of this study is limited access to large rainstorms throughout the growing season. Out of the seven largest rainstorms that occurred at Konza Prairie during the 2024 growing season, only one event (event number seven) was able to be analyzed, and our analysis only included two of our three study watersheds. These missed opportunities were majorly caused by availability of the research team and the unpredictability of large storm events in the Flint Hills region of Kansas. We recognize that the limits to the size of sampled storms decreases our ability to accurately characterize runoff generation mechanisms and differences in watershed behaviors due to woody plant encroachment. Nonetheless, the storms we did sample still allowed us to characterize concentrations over a significant range in discharge, and thus our analysis of concentration discharge (C-Q) relationships was not negatively impacted.

Additionally, this study could be greatly enhanced with the acquisition of more data such as evapotranspiration rates and soil saturation rates at the different watersheds surrounding a sampled precipitation event. Because woody plant species tend to transpire at greater rates than grass species (Keen et al., 2023; O'Keefe et al., 2020; Scott et al., 2006; J. Wang et al., 2018), knowing whole watershed evapotranspiration rates could help us better compare encroachments effects on streamflow sources and runoff generation. Woody plant encroachment can also decrease groundwater recharge because of the enhanced transpiration rates (Acharya et al., 2018), therefore direct measurements of soil saturation surrounding a sampled event could be valuable data. These two data measurements could help us better predict runoff generation likelihood, soil absorbance, and groundwater threshold within the different watersheds.

The primary limitation of this study is the lack of data collected on our watersheds as encroachment expanded over time. Ideally, we would have tracked changes in streamflow and solute sources over the past thirty years as encroachment progressed. Instead, we must infer the impacts of woody encroachment based on the current state of the watersheds. While this is a common approach, it introduces a degree of uncertainty. For instance, variations in subsurface flow pathways due to differences in bedrock fracture distribution and spacing could also explain the results observed in this study. We cannot definitively attribute the differences between watersheds to encroachment, as there may be unknown factors that existed beforehand.

Chapter 6 - Concluding Remarks

For this study, we conducted high-frequency sampling of three headwater catchments at the Konza Prairie Biological Station during seven different rainstorms during the 2024 water year to better understand and quantify the impacts woody plant encroachment has on streamflow sources and composition. Encroachment has the potential to alter soil permeability, increase infiltration, reduce runoff, dry near-surface soils, and even shift weathering processes deeper into the subsurface. Our hypothesis was that increased encroachment within a watershed would lead to a reduction in runoff generation and shift streamflow sources away from shallow soils while enhancing groundwater contributions.

Our analysis on stream responsiveness to storm events ($\Delta Q/P/A$ analysis) revealed that streams are becoming more responsive, potentially due to increases in storm intensity or other hydrological changes induced by climate change. We found that values of $\Delta Q/P/A$ increased for all three watersheds between the time intervals analyzed (1987-1990 and 2020-2023), but that the increase was greatest for the least encroached watershed, potentially reflecting the greater increases in soil permeability in the other watersheds as a result of greater encroachment. These observations potentially mean that encroachment is actually offsetting some of the effects of climate change by reducing stream responsiveness to storm events. This was further supported by our analysis examining how streamflow solutes behaved with changing discharge (C-Q analysis), where we observed the strongest mobilization behaviors in less encroached watersheds.

Moreover, we observed significant differences in the concentrations and mobilization of solutes that are vital to the wellbeing of many aquatic ecosystems and downstream water catchments. Woody plant encroachment's ability to increase pH, decrease alkalinity, and decrease the availability of crucial solutes at Konza Prairie could mean that grassland headwater catchments globally are being altered in similar ways. Additionally, we hypothesize that the removal of above ground riparian woody plant species may actually amplify the subsurface impacts of woody encroachment by combining the effects of legacy root systems with newly expanded woody plant species. This may extend the commonly held belief that once grasslands are replaced by woody encroachment, the effects are possibly irreversible and long withstanding. As woody encroachment erases our grassland ecosystems, it is vital to understand the processes, implications, and downstream affects it has on our ecosystems and water supply globally.

References

Acharya, B. S., Kharel, G., Zou, C. B., Wilcox, B. P., & Halihan, T. (2018). Woody Plant Encroachment Impacts on Groundwater Recharge: A Review. *Water*, *10*(10), 1466. https://doi.org/10.3390/w10101466

Anhold, C., Hatley, C., Alcantar-Velasquez, E., Keen, R. M., Sadayappan, K., Jarecke, K. M., Sullivan, P. L., Nippert, J. B., Li, L., Macpherson, G. L., & Kirk, M. F. (2025). Grassland woody encroachment alters subsurface mineral weathering and groundwater composition in a carbonate system. *Chemical Geology*, *673*, 122522. https://doi.org/10.1016/j.chemgeo.2024.122522

Blair, J., Nippert, J., & Briggs, J. (2014). Grassland Ecology. In R. K. Monson (Ed.), *Ecology and the Environment* (pp. 389–423). Springer New York. https://doi.org/10.1007/978-1-4614-7501-9_14

Bosch, J. M., & Hewlett, J. D. (1982). A review of catchment experiments to determine the effect of vegetation changes on water yield and evapotranspiration. *Journal of Hydrology*, *55*(1–4), 3–23. https://doi.org/10.1016/0022-1694(82)90117-2

Brookins, D. G., Chaudhuri, S., & Dowling, P. L. (1969). The isotopic composition of strontium in Permian limestones, eastern Kansas. *Chemical Geology*, *4*(3–4), 439–444. https://doi.org/10.1016/0009-2541(69)90009-6

Craig, H. (1961). Isotopic Variations in Meteoric Waters. *Science*, *133*(3465), 1702–1703. https://doi.org/10.1126/science.133.3465.1702

Dickson, T. L., Hayes, B. A., & Bragg, T. B. (2019). Effects of 34 Years of Experimentally Manipulated Burn Seasons and Frequencies on Prairie Plant Composition. *Rangeland Ecology & Management*, *72*(1), 82–91. https://doi.org/10.1016/j.rama.2018.07.014

Dodds, (2024a). *ASD02 Stream discharge measured at the flumes on watershed N04D at Konza Prairie* [Dataset]. Environmental Data Initiative. https://doi.org/10.6073/PASTA/C01278AAAAC74572EE53A4A6BA3017D3

Dodds, (2024b). *ASD04 Stream discharge measured at the flumes on watershed N20B at Konza Prairie* [Dataset]. Environmental Data Initiative. https://doi.org/10.6073/PASTA/A5EBF1B93505B2B09991A4201B5C87B3

Dodds, (2024c). *ASD05 Stream discharge measured at the flumes on watershed N01B at Konza Prairie* [Dataset]. Environmental Data Initiative. https://doi.org/10.6073/PASTA/7B75A0EFA4617F7D34DD9F2F583B686A

Dodds, Ratajczak, Z., Keen, R. M., Nippert, J. B., Grudzinski, B., Veach, A., Taylor, J. H., & Kuhl, A. (2023). Trajectories and state changes of a grassland stream and riparian zone after a decade of woody vegetation removal. *Ecological Applications*, *33*(4), e2830. https://doi.org/10.1002/eap.2830

Dodds, Robinson, C. T., Gaiser, E. E., Hansen, G. J. A., Powell, H., Smith, J. M., Morse, N. B., Johnson, S. L., Gregory, S. V., Bell, T., Kratz, T. K., & McDowell, W. H. (2012). Surprises and Insights from Long-Term Aquatic Data Sets and Experiments. *BioScience*, *62*(8), 709–721. https://doi.org/10.1525/bio.2012.62.8.4

Dore, M. H. I. (2005). Climate change and changes in global precipitation patterns: What do we know? *Environment International*, *31*(8), 1167–1181. https://doi.org/10.1016/j.envint.2005.03.004

Dugas, W. A., & Hicks, R. A. (n.d.). *Effect of removal of Juniperus ashei on evapotranspiration and runoff in the Seco Creek Watershed*. https://doi.org/10.1029/98WR00556

Hatley, C. M., Armijo, B., Andrews, K., Anhold, C., Nippert, J. B., & Kirk, M. F. (2023). Intermittent streamflow generation in a merokarst headwater catchment. *Environmental Science: Advances*, *2*(1), 115–131. https://doi.org/10.1039/D2VA00191H

Hayden, B. P. (1998). Regional Climate and the Distribution of Tallgrass Prairie. In A. K. Knapp, J. M. Briggs, D. C. Hartnett, & S. L. Collins (Eds.), *Grassland Dynamics* (pp. 19–34). Oxford University PressNew York, NY. https://doi.org/10.1093/oso/9780195114867.003.0002

Horton, R. E. (1933). The Role of infiltration in the hydrologic cycle. *Eos, Transactions American Geophysical Union*, *14*(1), 446–460. https://doi.org/10.1029/TR014i001p00446

Hulbert, L. (1985). *History and Use of Konza Prairie Research Natural Area from The Prairie Scout. 5*, 67–93.

Jarecke, K. M., Zhang, X., Keen, R. M., Dumont, M., Li, B., Sadayappan, K., Moreno, V., Ajami, H., Billings, S. A., Flores, A. N., Hirmas, D. R., Kirk, M. F., Li, L., Nippert, J. B., Singha, K., & Sullivan, P. L. (2025). Woody Encroachment Modifies Subsurface Structure and Hydrological Function. *Ecohydrology*, *18*(2), e2731. https://doi.org/10.1002/eco.2731

Keen, R. M., Nippert, J. B., Sullivan, P. L., Ratajczak, Z., Ritchey, B., O’Keefe, K., & Dodds, W. K. (2023). Impacts of Riparian and Non-riparian Woody Encroachment on Tallgrass Prairie Ecohydrology. *Ecosystems*, *26*(2), 290–301. https://doi.org/10.1007/s10021-022-00756-7

Keen, R. M., Sadayappan, K., Jarecke, K. M., Li, L., Kirk, M. F., Sullivan, P. L., & Nippert, J. B. (2024). Unexpected hydrologic response to ecosystem state change in tallgrass prairie. *Journal of Hydrology*, *643*, 131937. https://doi.org/10.1016/j.jhydrol.2024.131937

Kharel, G., Zou, C., Wilcox, B., & Halihan, T. (2018). Woody Plant Encroachment Impacts on Groundwater Recharge: A Review. *Water*, *10*(10), 1466. https://doi.org/10.3390/w10101466

Kirk, M., & Macpherson, G. (2024). *AGW01 Long-term measurement of groundwater physical and chemical properties from wells on watersheds N04D and N01B at Konza Prairie* [Dataset]. Environmental Data Initiative. https://doi.org/10.6073/PASTA/1247B3E5935928B350572E011917155F

Klaus, J., & McDonnell, J. J. (2013). Hydrograph separation using stable isotopes: Review and evaluation. *Journal of Hydrology*, *505*, 47–64. https://doi.org/10.1016/j.jhydrol.2013.09.006

Lapides, D. A., Leclerc, C. D., Moidu, H., Dralle, D. N., & Hahm, W. J. (2021). Variability of stream extents controlled by flow regime and network hydraulic scaling. *Hydrological Processes*, *35*(3), e14079. https://doi.org/10.1002/hyp.14079

Li, L. (2019). Watershed Reactive Transport. *Reviews in Mineralogy and Geochemistry*, *85*(1), 381–418. https://doi.org/10.2138/rmg.2018.85.13

Li, L., Stewart, B., Zhi, W., Sadayappan, K., Ramesh, S., Kerins, D., Sterle, G., Harpold, A., & Perdrial, J. (2022). Climate Controls on River Chemistry. *Earth's Future*, *10*(6), e2021EF002603. https://doi.org/10.1029/2021EF002603

Macpherson, G. L. (1996). Hydrogeology of thin limestones: The Konza Prairie Long-Term Ecological Research Site, Northeastern Kansas. *Journal of Hydrology*, *186*(1–4), 191–228. https://doi.org/10.1016/S0022-1694(96)03029-6

Macpherson, G. L., Roberts, J. A., Blair, J. M., Townsend, M. A., Fowle, D. A., & Beisner, K. R. (2008). Increasing shallow groundwater CO2 and limestone weathering, Konza Prairie, USA. *Geochimica et Cosmochimica Acta*, *72*(23), 5581–5599. https://doi.org/10.1016/j.gca.2008.09.004

Macpherson, G. L., & Sullivan, P. L. (2019). Dust, impure calcite, and phytoliths: Modeled alternative sources of chemical weathering solutes in shallow groundwater. *Chemical Geology*, *527*, 118871. https://doi.org/10.1016/j.chemgeo.2018.08.007

Marvel, K., Su, W., Delgado, R., Aarons, S., Chatterjee, A., Garcia, M. E., Hausfather, Z., Hayhoe, K., Hence, D. A., Jewett, E. B., Robel, A., Singh, D., Tripati, A., Vose, R. S., Crimmins, A. R., Avery, C. W., Easterling, D. R., Kunkel, K. E., Stewart, B. C., & Maycock, T. K. (2023). *Chapter 2: Climate Trends. Fifth National Climate Assessment*. U.S. Global Change Research Program. https://doi.org/10.7930/NCA5.2023.CH2

Nippert, J. (2024). *APT01 Daily precipitation amounts measured at multiple sites across konza prairie* [Dataset]. Environmental Data Initiative. https://doi.org/10.6073/PASTA/E9C078D2C7EA9DBFE72F22718DC2E72E

O’Keefe, K., Bell, D. M., McCulloh, K. A., & Nippert, J. B. (2020). Bridging the Flux Gap: Sap Flow Measurements Reveal Species-Specific Patterns of Water Use in a Tallgrass Prairie. *Journal of Geophysical Research: Biogeosciences*, *125*(2), e2019JG005446. https://doi.org/10.1029/2019JG005446

O'Keefe, K., Nippert, J. B., & McCulloh, K. A. (2019). Plant water uptake along a diversity gradient provides evidence for complementarity in hydrological niches. *Oikos*, *128*(12), 1748–1760. https://doi.org/10.1111/oik.06529

Oviatt, C. G. (1998). Geomorphology of the Konza Prairie. *Grassland Dynamics: Long-Term Ecological Research in Tallgrass Prairie.*, 35–47.

Pruitt, J., & Kirk, M. (2025). *AGW04 Measurement of stream chemical properties during growing season rainfall events at konza prairie, 2024* [Dataset].

Qiao, L., Zou, C. B., Stebler, E., & Will, R. E. (2017). Woody plant encroachment reduces annual runoff and shifts runoff mechanisms in the tallgrass prairie, U SA. *Water Resources Research*, *53*(6), 4838–4849. https://doi.org/10.1002/2016WR019951

Ratajczak, Z., Nippert, J. B., Hartman, J. C., & Ocheltree, T. W. (2011). Positive feedbacks amplify rates of woody encroachment in mesic tallgrass prairie. *Ecosphere*, *2*(11), art121. https://doi.org/10.1890/ES11-00212.1

Saalidong, B. M., Aram, S. A., Otu, S., & Lartey, P. O. (2022). Examining the dynamics of the relationship between water pH and other water quality parameters in ground and surface water systems. *PLOS ONE*, *17*(1), e0262117. https://doi.org/10.1371/journal.pone.0262117

Sadayappan, K., Keen, R., Jarecke, K. M., Moreno, V., Nippert, J. B., Kirk, M. F., Sullivan, P. L., & Li, L. (2023). Drier streams despite a wetter climate in woody-encroached grasslands. *Journal of Hydrology*, *627*, 130388. https://doi.org/10.1016/j.jhydrol.2023.130388

Scholl, M. (2018). *Precipitation isotope collector designs*.

Scott, R. L., Huxman, T. E., Williams, D. G., & Goodrich, D. C. (2006). Ecohydrological impacts of woody-plant encroachment: Seasonal patterns of water and carbon dioxide exchange within a semiarid riparian environment. *Global Change Biology*, *12*(2), 311–324. https://doi.org/10.1111/j.1365-2486.2005.01093.x

Speir, S. L., Rose, L. A., Blaszczak, J. R., Kincaid, D. W., Fazekas, H. M., Webster, A. J., Wolford, M. A., Shogren, A. J., & Wymore, A. S. (2023). Catchment concentration–discharge relationships across temporal scales: A review. *WIREs Water*, e1702. https://doi.org/10.1002/wat2.1702

Steenhuis, T. S., Mukundan, R., & Tilahun, S. A. (2023). Overland flow. In M. J. Goss & M. Oliver (Eds.), *Encyclopedia of Soils in the Environment (Second Edition)* (pp. 287–293). Academic Press. https://doi.org/10.1016/B978-0-12-822974-3.00163-4

Steward, D. R., Yang, X., Lauwo, S. Y., Staggenborg, S. A., Macpherson, G. L., & Welch, S. M. (2011). From precipitation to groundwater baseflow in a native prairie ecosystem: A regional study of the Konza LTER in the Flint Hills of Kansas, USA. *Hydrology and Earth System Sciences*, *15*(10), 3181–3194. https://doi.org/10.5194/hess-15-3181-2011

Stewart, B., Shanley, J. B., Kirchner, J. W., Norris, D., Adler, T., Bristol, C., Harpold, A. A., Perdrial, J. N., Rizzo, D. M., Sterle, G., Underwood, K. L., Wen, H., & Li, L. (2022). Streams as Mirrors: Reading Subsurface Water Chemistry From Stream Chemistry. *Water Resources Research*, *58*(1), e2021WR029931. https://doi.org/10.1029/2021WR029931

Sullivan, P. L., Macpherson, G. L., Martin, J. B., & Price, R. M. (2019). Evolution of carbonate and karst critical zones. *Chemical Geology*, *527*, 119223. https://doi.org/10.1016/j.chemgeo.2019.06.023

Sullivan, P. L., Stops, M. W., Macpherson, G. L., Li, L., Hirmas, D. R., & Dodds, W. K. (2019). How landscape heterogeneity governs stream water concentration-discharge behavior in carbonate terrains (Konza Prairie, USA). *Chemical Geology*, *527*, 118989. https://doi.org/10.1016/j.chemgeo.2018.12.002

Swenson, L. J., Zipper, S., Peterson, D. M., Jones, C. N., Burgin, A. J., Seybold, E., Kirk, M. F., & Hatley, C. (2024). Changes in Water Age During Dry-Down of a Non-Perennial Stream. *Water Resources Research*, *60*(1), e2023WR034623. https://doi.org/10.1029/2023WR034623

Swindle, C., Shankin-Clarke, P., Meyerhof, M., Carlson, J., & Melack, J. (2021). Effects of Wildfires and Ash Leaching on Stream Chemistry in the Santa Ynez Mountains of Southern California. *Water*, *13*(17), 2402. https://doi.org/10.3390/w13172402

Tsypin, M., & Macpherson, G. L. (2012). The effect of precipitation events on inorganic carbon in soil and shallow groundwater, Konza Prairie LTER Site, NE Kansas, USA. *Applied Geochemistry*, *27*(12), 2356–2369. https://doi.org/10.1016/j.apgeochem.2012.07.008

Veach, A. M., Dodds, W. K., & Skibbe, A. (2014). Fire and Grazing Influences on Rates of Riparian Woody Plant Expansion along Grassland Streams. *PLoS ONE*, *9*(9), e106922. https://doi.org/10.1371/journal.pone.0106922

Vero, S. E., Macpherson, G. L., Sullivan, P. L., Brookfield, A. E., Nippert, J. B., Kirk, M. F., Datta, S., & Kempton, P. (2018). Developing a Conceptual Framework of Landscape and Hydrology on Tallgrass Prairie:A Critical Zone Approach. *Vadose Zone Journal*, *17*(1), 1–11. https://doi.org/10.2136/vzj2017.03.0069

Wang, D., Tian, L., Risi, C., Wang, X., Cui, J., Bowen, G. J., Yoshimura, K., Wei, Z., & Li, L. Z. X. (2023). Vehicle-based in situ observations of the water vapor isotopic composition across China: Spatial and seasonal distributions and controls. *Atmospheric Chemistry and Physics*, *23*(6), 3409–3433. https://doi.org/10.5194/acp-23-3409-2023

Wang, J., Xiao, X., Zhang, Y., Qin, Y., Doughty, R. B., Wu, X., Bajgain, R., & Du, L. (2018). Enhanced gross primary production and evapotranspiration in juniper-encroached grasslands. *Global Change Biology*, *24*(12), 5655–5667. https://doi.org/10.1111/gcb.14441

Wilcox, B. P. (2002). Shrub Control and Streamflow on Rangelands: A Process Based Viewpoint. *Journal of Range Management*, *55*(4), 318. https://doi.org/10.2307/4003467

Wilcox, B. P., Owens, M. K., Dugas, W. A., Ueckert, D. N., & Hart, C. R. (2006). Shrubs, streamflow, and the paradox of scale. *Hydrological Processes*, *20*(15), 3245–3259. https://doi.org/10.1002/hyp.6330

Wood, H. K., & Macpherson, G. L. (2005). Sources of Sr and implications for weathering of limestone under tallgrass prairie, northeastern Kansas. *Applied Geochemistry*, *20*(12), 2325–2342. https://doi.org/10.1016/j.apgeochem.2005.08.002

Zhu, G., Zhang, Z., Guo, H., Zhang, Y., Yong, L., Wan, Q., Sun, Z., & Ma, H. (2021). Below-Cloud Evaporation of Precipitation Isotopes over Mountains, Oases, and Deserts in Arid Areas. *Journal of Hydrometeorology*, *22*(10), 2533–2545. https://doi.org/10.1175/JHM-D-20-0170.1

Appendix A - Concentration-Discharge Data

N1B	b	mean C	mean Q	standard dev C	standard dev Q	Coefficients
Fluoride	-0.03530206	0.41247312	0.00481548	0.038049908	0.003114012	0.14265191
Chloride	0.11099365	2.70667742	0.00481548	0.512788459	0.003114012	0.2929688
Alkalinity	0.04072582	5.50010753	0.00481548	0.533457742	0.003114012	0.14998522
Sulfate	-0.12686243	21.6265054	0.00481548	2.703373085	0.003114012	0.1933033
Sodium	-0.07759908	4.77497849	0.00481548	0.470324171	0.003114012	0.152316
Potassium	-0.02773712	0.97082796	0.00481548	0.133089511	0.003114012	0.21199284
Magnesium	-0.03938538	16.4426452	0.00481548	0.787164002	0.003114012	0.07403092
Calcium	0.04794825	90.011871	0.00481548	11.72723718	0.003114012	0.2014724
Strontium	-0.06529061	4.081125	0.00481548	0.515753719	0.003114012	0.19542589

N2B	b	mean C	mean Q	standard dev C	standard dev Q	Coefficients
Fluoride	-0.057069057	0.367202381	0.006865429	0.030588517	0.012065172	0.047400951
Chloride	-0.039879092	2.345321429	0.006865429	0.47534082	0.012065172	0.115328558
Alkalinity	-0.024057854	5.340083333	0.006865429	0.478114772	0.012065172	0.050946957
Sulfate	-0.126051717	18.04564286	0.006865429	2.953346024	0.012065172	0.093127104
Sodium	-0.13559396	3.606452381	0.006865429	0.624827136	0.012065172	0.098585673
Potassium	0.141619171	1.039964286	0.006865429	0.396890184	0.012065172	0.217163112
Magnesium	-0.086048689	15.05055952	0.006865429	1.818179716	0.012065172	0.068741386
Calcium	-0.023386319	88.22090476	0.006865429	14.08537188	0.012065172	0.090851256
Strontium	-0.091524966	3.509571429	0.006865429	0.50999092	0.012065172	0.082687999

N4D	b	mean C	mean Q	standard dev C	standard dev Q	Coefficients
Fluoride	-0.070222238	0.398946667	0.023586053	0.046669885	0.045938787	0.060061704
Chloride	-0.084420008	1.968666667	0.023586053	0.521600793	0.045938787	0.136032227
Alkalinity	-0.042416149	4.78768	0.023586053	0.677604867	0.045938787	0.072665314
Sulfate	-0.308272706	18.73428	0.023586053	4.655779113	0.045938787	0.127594253
Sodium	-0.21013728	4.004493333	0.023586053	0.728149884	0.045938787	0.093357446
Potassium	0.2445009	1.044586667	0.023586053	0.57029445	0.045938787	0.280304726
Magnesium	-0.138527394	16.78944	0.023586053	2.377542834	0.045938787	0.072705605
Calcium	-0.036061809	71.36158667	0.023586053	14.71138717	0.045938787	0.105843668
Strontium	-0.106844259	3.630523077	0.023586053	0.48753481	0.045938787	0.068946493

Appendix B – 2024 Precipitation-Discharge Data

	N1B				
	P (mm)	P (m)	aQ (m^3/s)	dQ (m^3/s)	(dQ)/(P)/A
4/25/24	64.2	0.064	0.000	5.363	6.96E-05
5/2/24	10.4	0.010	0.007	0.004	3.45E-07
5/4/24	11.2	0.011	0.006	0.193	1.44E-05
5/13/24	32.0	0.032	0.003	0.006	1.44E-07
5/19/24	43.2	0.043	0.005	1.332	2.57E-05
5/26/24	35.4	0.035	0.012	1.034	2.43E-05
6/2/24	7.6	0.008	0.008	0.003	3.09E-07
6/6/24	5.8	0.006	0.005	0.001	1.89E-07
6/16/24	50.0	0.050	0.000	0.008	1.28E-07
6/28/24	48.2	0.048	0.000	0.356	6.15E-06
7/1/24	52.2	0.052	0.000	1.552	2.48E-05
7/4/24	30.0	0.030	0.007	3.760	1.04E-04
7/16/24	21.2	0.021	0.002	0.012	4.72E-07

	N2B				
	P* (mm)	P* (m)	aQ (m^3/s)	dQ (m^3/s)	(dQ)/(P)/A
4/25/24	61.8	0.062	0.000	0.729	9.91E-06
5/2/24	10.0	0.010	0.006	0.004	3.05E-07
5/4/24	15.0	0.015	0.006	0.021	1.19E-06
5/6/24	3.4	0.003	0.006	0.001	2.41E-07
5/13/24	23.4	0.023	0.003	0.003	1.23E-07
5/19/24	42.6	0.043	0.001	0.039	7.61E-07
5/26/24	39.8	0.040	0.002	0.080	1.70E-06
6/2/24	9.4	0.009	0.003	0.002	1.68E-07
6/6/24	6.2	0.006	0.001	0.001	1.36E-07
7/1/24	49.6	0.050	0.000	0.179	3.04E-06
7/4/24	26.6	0.027	0.001	0.156	4.93E-06
7/16/24	23.6	0.024	0.000	0.012	4.36E-07

	N4D				
	P (mm)	P (m)	aQ (m^3/s)	dQ (m^3/s)	(dQ)/(P)/A
4/25/24	61.8	0.062	0.000	2.043	2.45E-05
5/2/24	10.0	0.010	0.021	0.008	5.63E-07
5/4/24	15.0	0.015	0.018	0.028	1.38E-06
5/6/24	3.4	0.003	0.023	0.003	5.88E-07
5/13/24	23.4	0.023	0.012	0.009	2.98E-07
5/19/24	42.6	0.043	0.012	0.313	5.44E-06
5/26/24	39.8	0.040	0.015	0.333	6.20E-06
6/2/24	9.4	0.009	0.017	0.005	3.55E-07
6/6/24	6.2	0.006	0.010	0.001	1.19E-07
6/9/24	6.4	0.006	0.008	0.002	2.08E-07
6/16/24	44.2	0.044	0.005	0.023	3.80E-07
6/19/24	19.4	0.019	0.003	0.003	9.55E-08
6/28/24	43.8	0.044	0.000	0.383	6.47E-06
7/1/24	49.6	0.050	0.004	0.547	8.17E-06
7/4/24	26.6	0.027	0.018	0.763	2.12E-05
7/16/24	23.6	0.024	0.009	0.031	9.86E-07
7/31/24	29.6	0.030	0.001	0.009	2.34E-07

Appendix C – Surface Water Geochemistry Calculations

	Mean			Median		
	N01B	N02B	N04D	N01B	N02B	N04D
pH	7.65	7.67	7.84	7.56	7.68	7.84
Temp	16.37	16.66	18.14	16.17	16.56	18.41
Alk	5.54	5.34	4.79	5.68	5.55	4.89
F-	0.42	0.37	0.40	0.42	0.37	0.42
Cl-	2.71	2.35	1.97	2.52	2.30	1.91
SO4-2	21.65	18.05	18.73	21.89	18.88	19.14
Na+	4.78	3.61	4.00	4.91	3.73	4.16
K+	0.97	1.04	1.04	0.95	0.91	0.85
Mg2+	16.44	15.05	16.79	16.39	15.25	17.50
Ca2+	90.84	88.61	71.36	93.55	92.24	71.99
Sr2+	4.14	3.51	3.63	4.18	3.66	3.75
NPOC	1.84	2.04	2.27	1.78	1.69	1.55
TN	0.21	0.18	0.19	0.19	0.15	0.15

	Standard Deviation			*p*-value		
	N01B	N02B	N04D	N01B & N02B	N01B & N04D	N02B & N04D
pH	0.17	0.07	0.07	2.90E-01	3.18E-16	2.39E-33
Temp	2.27	1.86	2.41	3.46E-01	2.32E-06	2.27E-05
Alk	0.37	0.66	0.68	1.53E-02	4.73E-16	5.44E-07
F-	0.02	0.03	0.05	2.47E-23	3.81E-03	8.71E-07
Cl-	0.52	0.48	0.52	2.67E-06	1.66E-16	4.29E-06
SO4-2	2.71	2.95	4.66	1.08E-14	1.12E-06	2.62E-01
Na+	0.47	0.62	0.73	1.56E-30	4.71E-14	2.88E-04
K+	0.13	0.40	0.57	1.22E-01	2.38E-01	9.52E-01
Mg2+	0.79	1.82	2.38	2.94E-10	1.92E-01	5.83E-07
Ca2+	8.66	13.70	14.71	1.95E-01	1.85E-20	1.88E-12
Sr2+	0.33	0.51	0.49	5.95E-10	1.12E-08	2.21E-01
NPOC	0.40	1.17	2.44	1.32E-01	9.65E-02	4.31E-01
TN	0.19	0.08	0.12	9.15E-02	3.42E-01	4.25E-01